SRF Kanpur
PUBLICATIONS...

Publisher

Social Research Foundation
128/170, H-Block, Kidwai Nagar, Kanpur-11
9335332333, 9839074762
www.socialresearchfoundation.com

ISBN

9 789393 166838

Price : 499 INR

Ceramic Glasses * Dr. Samay Singh Meena

ISBN : 978-93-93166-83-8

CERAMIC GLASSES

2024

DR. SAMAY SINGH MEENA

Ceramic Glasses

Author

Dr. Samay Singh Meena
Assistant Professor
Department of Physics
Jai Narain Vyas University
Jodhpur, Rajasthan, India

Publisher

Social Research Foundation
128/170, H-Block, Kidwai Nagar, Kanpur-11
Uttar Pradesh, India
9335332333, 9839074762

Title	**:**	**Ceramic Glasses**
Author	:	Dr. Samay Singh Meena
Publisher	:	Social Research Foundation
Publisher Address	:	128/170, H-Block, Kidwai Nagar, Kanpur, Uttar Pradesh, India
Printer's Detail	:	Social Research Foundation
Printer's Address	:	128/170, H-Block, Kidwai Nagar, Kanpur, Uttar Pradesh, India
Edition	:	1st Edition, 2024
ISBN	:	978-93-93166-83-8
DOI	:	10.5281/zenodo.13751889
Cover Clips Source	:	Internet
Copyright © Publisher		
Price	:	499 INR

Preface

I Feel great pleasure in bringing out the first coliseum of the book" ceramic glasses ". This book has been designed strictly according to the unified syllabus of Rajasthan state Universities and colleges students. A reasonable wide coverage in sufficient depth has been attempted. To clearly the concepts and for making varying standards are incorporated.

In writing this book, I have tried to present the subject matter in a simple tonguage so that an average student feels interesting in the following text .I have also kept in mind that after studying this book, the base of knowledge of the students become so strong that they may not feel difficulty in understanding the subject matter in higher classes a hope that if a student goes through serious by with this book, he or she would appreciate and enjoy the subject.

I thankful to our near dear ones for their blessings, good wishes and co-operations due to which the implementation of this project could become possible.

I also thankful to the publisher, typesetter, printer, proof-readers and numerous others did their relevant work with complete improvement and dedication. In spite of great cane, some misprints and condescension might have crept in. I will be thankful to readers who will point out and inform any mistake further any suggestions towards the improvement of subject matter will be thankful received.

Dr. Samay Singh Meena

INDEX

CHAPTER 1

INTRODUCTION

Glass-ceramics are polycrystalline materials produced through controlled crystallization of base glass, producing a fine uniform dispersion of crystals throughout the bulk material. Crystallization is accomplished by subjecting suitable glasses to a carefully regulated heat treatment schedule, resulting in the nucleation and growth of crystal phases. In many cases, the crystallization process can proceed to near completion, but in a small proportion of processes, the residual glass phase often remains.

Glass-ceramic materials share many properties with both glasses and ceramics. Glass-ceramics have an amorphous phase and one or more crystalline phases and are produced by a so-called "controlled crystallization" in contrast to a spontaneous crystallization, which is usually not wanted in glass manufacturing. Glass-ceramics have the fabrication advantage of glass, as well as special properties of ceramics. When used for sealing, some glass-ceramics do not require brazing but can withstand brazing temperatures up to 700 °C. Glass-ceramics usually have between 30% and 90% crystallinity and yield an array of materials with interesting properties like zero porosity, high strength, toughness,

translucency or opacity, pigmentation, opalescence, low or even negative thermal expansion, high temperature stability, fluorescence machinability, ferromagnetism, restorability or high chemical durability, biocompatibility, bioactivity, ion conductivity, superconductivity, isolation capabilities, low dielectric constant loss, corrosion resistance, high resistivity and break-down voltage. These properties can be tailored by controlling the base-glass composition and by controlled heat treatment/crystallization of base glass. In manufacturing, glass-ceramics are valued for having the strength of ceramic but the hermetic sealing properties of glass.

The history of glasses and amorphous materials are back to very beginning of almost all the civilization in the world. These materials found their applications as the decorating materials and in pottery. From electronic and technological point of view these materials have recently attracted the attention of scientific community. These materials were believed to be insulators in general. On the absence of long-range order these materials were believed to be semiconductors. Structural materials greatly depend upon the technique adopted.

During 50^{th} and 60^{th} this field again caught the attention of research workers because of the pioneer works in the experimental field. Very interesting properties of materials have been investigated semiconducting properties photoconduction properties, switching properties, memory retention properties have been found in these materials High

temperature superconducting properties of the amorphous materials have also been investigated. Now a day's these materials find their application in amorphous solar cells and devices for conversion of solar energy into usable form of energy.

S, Se, Te elements of the groups VI of the periodic table are called chalcogen atoms. Amorphous materials which contain one of the above elements as the constituent are termed as chalcogenide glasses.

Properties of chalcogenide glasses are: -

1. It was believed that these chalcogenides glasses are generally insensitive to the incorporation of impurities.
2. Fermi level is pinned near mid gap.
3. General p- type conduction in these materials is observed.
4. General similarities in the overall distribution of the corresponding crystalline phase states.

At present glass is a versatile material that is commercially available over a wide range of compositions which can be fabricated by several techniques to produce variety of photonic devices. They can be manufactured with excellent homogeneity and without gain boundaries easily in different desired forms. That is Prisms, flats, lenses and optical fibers. The RE doped glasses have gained popularities for use in solid state lasers and optical amplifiers. They can also be used as sensors in industrial process control, high temperature monitoring of electrical power stations, oil refineries and coli mines.

In glassy materials, the three-dimensional random network of strong bonds is formed by the constituents of the so called 'network former'. To incorporate a foreign ion into such a structure, one often needs the addition of certain other compounds i.e. Alkali oxides, alkali fluoride, lead oxide, and fluorides etc. termed as "network modifiers". Their introduction breaks the glass network at several places, where the foreign ions can enter. The modified structure becomes loose and therefore, even permits easy ion migration.

Most of the glasses exhibit the decrease in specific volume with the defining of temperature. Following is some of the significant physical properties of glasses -

1. Glasses are said to be isotropic, because their physical properties are uniform in all directions.
2. They have short range atomic order.
3. Glasses are electrically and thermally insulating at normal temperatures, but become conducting at elevated temperatures.
4. Glasses soften before melting, so they can be formed by various glass form techniques.
5. The density, elastic constants, specific heat dielectric permittivity are compositions dependent.

Rare earth ions doping spectroscopy

When RE ions are doped in any host material, they form optically active centers and exhibit luminescence when exhibits by an appropriate excitation source. The RE ions exist in the solid matrices either as RE^{3+} or RE^{2+} ions with their electronics configuration as $4f^n$ 5s $5p^6$ or $4f^{n-1}$ 5s $5p^6$

respectively. Therefore, the trivalent lanthanide ions have a xenon core electronic configuration, with the addition of $4f^n$ electrons, [Xe] $4f^n$, where 'n' varies progressively from 0 to 14.

General properties of RE ions

Generally, the energy levels of RE^{3+} ions do not change greatly with host i.e. if a given ion is demonstrated to lase in one host, there are usually many other host possibilities following are the general properties that are commonly shared by the REs.

1. They can easily burn in air.
2. Their hardness slightly increases with increase atomic number.
3. RE ions possess high melting and boiling points.
4. Their compounds are generally ionic.
5. They are strong reducing agents.
6. They react with water to liberate hydrogen (H), slowly in cold and quickly upon heating.
7. Lanthanide compounds are strongly paramagnetic (except La^{3+} and Lu^{3+}).
8. The coordination number of lanthanides are (greater than 6: usually 8 or 9 as high as 12).

Emission colors of RE ions

The 4f-4f transitions occurring in the visible region of the spectrum are responsible for the characteristic color of the RE ions. Main-Smith tried to correlate the color sequence in RE series with the 4f electronic configuration of the RE^{3+} ions. The characteristics colors of the RE^{3+} ions are caused by the

internal transitions of the 4f electrons, occurring in the visible region of the spectrum.

Optical properties of rare earth ions-

Following are some of the optical properties which make RE^{3+} ions as favorable candidates for luminescent device fabrication –

1. Luminescence of RE^{3+} ions spreads in the various spectral images.
2. They have long emission lifetimes.
3. They have small homogenous line widths.
4. They possess high refraction with relatively low dispersion.
5. There have several excited states suitable for optical pumping.

Applications of RE ions in glasses-

The usage of RE elements in glass technology has revealed several scientific and technological applications as follows –

1. Communication fibers and glass fibers.
2. LED and color television phosphors.
3. Optical glasses, fibers and lenses.
4. Light sensitive and photochromic glasses.
5. Coloring and decoloring agents.
6. Glass polishing agents.
7. PH – electrodes.
8. X-ray and Y- ray absorbing glasses.

CHAPTER 2

CLASSIFICATION OF CERAMIC GLASSES

Glass-ceramics are polycrystalline materials produced through controlled crystallization of base glass, producing a fine uniform dispersion of crystals throughout the bulk material. Crystallization is accomplished by subjecting suitable glasses to a carefully regulated heat treatment schedule, resulting in the nucleation and growth of crystal phases. In many cases, the crystallization process can proceed to near completion, but in a small proportion of processes, the residual glass phase often remains. Natural glasses were formed in the earth's crust or in meteorites or lunar rocks. Most important natural glasses are tektite and obsidian. Some other types are basaltic deep-sea glass and fractionate glass.

Although most people think of glass as a man-made material, it is found in many forms in the natural world. Volcanoes spew molten rock, lightning strikes desert and beach sands, meteorites pound the earth, and sea sponges and microscopic organisms inhabit the waters.

Glass is made from raw materials found in nature, such as sand, soda ash and limestone, as well as recycled glass (known as cullet). These raw materials are locally and sustainably sourced, respecting the planet's ecosystems and

complying with strict specifications. Ceramic glasses are basically two types; Natural glass and artificial glass.

2.1 Normal ceramic glass: The making of glass is a skilled labor and exquisite art; by human hands for many a century, but Nature has been doing so for millions of years. To show some examples of this, here are ten types of natural glass that are found throughout the world.

2.1.1 Tektite: Tektite occurs when a large meteor impact strikes sandy ground. If the sand is nearly pure silica, then it is known as Lechatelierite (though this is not the only way Lechatelierite forms). The vast majority of Tektites are black and can be mistaken for Obsidian by untrained eyes.

2.1.2 Libyan Desert Glass: Libyan Desert Glass is a form of Lechatelierite found in the western Egypt and Libya regions of the Sahara, with a large sum of specimens found at Kebira Crater (this being the source of LDG is disputed). LDG was formed ~29 million years ago, either from a meteor impact or an airburst, the latter of which is a meteor or comet that exploded in Earth's atmosphere rather than striking the surface.

2.1.3 Moldavite: Moldavite is a green Tektite primarily found in southern Bohemia, Czechia that formed ~15 million years ago. Occasional specimens contain squiggly streaks of Lechatelierite.

2.1.4 Georgiaite: Georgiaite is a dark olive-green Tektite that formed ~35 million years ago and found only in the U.S. state of Georgia. It's just shy of qualifying as a Lechatelierite because it contains potassium but no other impurities.

2.1.5 Atacama Desert Glass: Atacama Desert Glass is named after the area in which it is found in northern Chile. Rather than from a meteor impact, this natural glass formed by the occurrence of an airburst, in particular a comet exploded above the region ~12,000 years ago. Most ADG specimens are black, though some are dark green.

2.1.6 Edeowie: Edeowie is a natural glass found in the Australian state of South Australia. Its origins are unknown; the top three suspects are meteor impact, lightning strikes, or high temperature grassland fires. Colors range from black to a greyish green.

2.1.7 Darwin Glass: Darwin Glass is a natural glass found in Darwin Crater in Tasmania, Australia. Though the crater is likely a meteor impact one, it hasn't been conclusively confirmed, which is why the glass is not labelled as a Tektite. Its colors range from white to black, with many hues of green in-between.

2.1.8 Fulgurite: Fulgurite, also known as Fossilized Lightning, can occur anyplace lightning has struck

sandy ground. If the stricken sand is almost 100% silica, then it also qualifies as a Lechatelierite.

2.1.9 Trinitite: Trinitite, also known as Atomsite or Alamogordo Glass, is an artificial glass formed from the Trinity Nuclear Bomb Test in New Mexico in 1945. Though mildly radioactive, it's considered safe to handle, however that didn't stop the U.S. government from barring any further collection of specimens on threat of fines and jail time. Sometimes the term "Trinitite" is used to describe all nuke-formed glass. (The reason this is listed is because although it only formed due to human actions, the main materials were natural, and the production was very similar to what happens during a meteor impact).

2.1.10 Obsidian: Obsidian is likely the most well-known natural glass on this list, as it is often shown as an example of volcanic activity in grade school science classes. Obsidian can be found worldwide at both active and dormant volcanoes, though not all produce this glass- only volcanoes that eject the highly viscous felsic lava, which is rich in silica (the same chemical makeup as sand and quartz). Just as there are many types of Tektites, there are several different forms of Obsidian.

2.2 Artificial Ceramic glasses: Human made ceramic glasses known as artificial glass. They are sub categorized as; Oxide glasses- silicate, borate, phosphate, and germinate glasses. Halide glasses- Bef is a glass network former. Fluorozirconate, fluoroborates and flurophosphate glasses. Chalcogenides glasses- these glasses are prepared based on elements of group of VI(S, Se, Te) combined with elements of group IV(Si & Ge) and group of V(P, As, Sb, Bi) which do not contain oxygen are interesting due to their infrared optical transmission & electrical switching properties. Metallic glasses- metal-metalloid alloys and metal- metal alloys.

2.2.1 Silicate glass: Silicate glasses are historically the oldest types of glasses which were manufactured by human beings, and are still the most common glasses. They largely consist of silicon dioxide (silica, SiO_2), but in contrast to pure silica glass they contain some additional substances like soda, alumina, phosphorus pentoxide, Germania and potassium carbonate.

2.2.2 Phosphate glass: Phosphate glass is a class of optical glasses composed of metaphosphates of various metals. Instead of SiO_2 in silicate glasses, the glass forming substrate is P_2O_5. P_2O_5 crystallizes in at least four forms. The most familiar polymorph comprises molecules of P_4O_{10}. The other polymorphs are

polymeric, but in each case the phosphorus atoms are bound by a tetrahedron of oxygen atoms, one of which forms a terminal P=O bond. The O-form adopts a layered structure consisting of interconnected P_6O_6 rings, not unlike the structure adopted by certain polyciliate.

2.2.3 Borate glass: Borate glasses have a more complex action of alkali ions than silicate glasses. Borate glasses also have major differences in their optical properties. The single largest use of boron compounds in the world (accounting for half of total global use) is the production of certain types of boron-treated glass Fiber for insulating and structural fiberglass. In these uses the boron may be present as borax or boron oxide, and adds to the structural strength of the glass as borosilicate, or is added as a fluxing agent to decrease the melting temperature of pure silica, which is difficult to extrude as fibers and work with in pure form, due to the high temperatures involved.

2.2.4 Tellurite glass: Tellurite glass is a type of glass material that is composed primarily of tellurium dioxide (TeO_2) along with other elements such as silicon dioxide (SiO_2) and metal oxides. It is known for its low host phonon energy and the ability to form unique nanostructured crystalline phases upon crystallization. The composition of tellurite glass can

be modified to achieve different crystalline phases with unique structures and properties. It has been studied for its potential applications in photonics, including as a material for radiation shielding. Tellurite glass can also be used to fabricate microbubble whispering gallery resonators (WGRs) with high quality factors and a wide range of optical characteristics. Understanding the thermal properties and coordination numbers of alkali and alkaline earth tellurite glasses can provide insights into the structure of amorphous TeO_2.

2.2.5 Halide glass: Halide glasses are made of inorganic halide (e.g., fluoride (F^-), chloride (Cl^-), bromide (Br^-), and iodide (I^-) salts. Heavy metal halides (HMH) are the major constituents of this family of glasses. The glass systems ZrF_4–BaF_2–LaF_3–AlF_3 (ZBLA), ZrF_4–BaF_2–LaF_3–AlF_3–NaF (ZBLAN), ZrF_4–BaF_2–YF_3–AlF_3 (ZBYA) etc.

2.2.6 Chalcogenide glass: Chalcogenide glass is a glass containing one or more chalcogens (sulphur, selenium and tellurium, but excluding oxygen). Polonium is also a chalcogen but is not used because of its strong radioactivity. Chalcogenide materials behave rather differently from oxides, in particular their lower band gaps contribute to very dissimilar optical and electrical properties. The classical chalcogenide glasses (mainly sulfur-based ones such as As-S or Ge-S) are

strong glass-formers and possess glasses within large concentration regions. Glass-forming abilities decrease with increasing molar weight of constituent elements; i.e., S > Se > Te. Chalcogenide compounds such as AgInSbTe and GeSbTe are used in rewritable optical and phase-change memory devices. They are fragile glass-formers: by controlling heating and annealing (cooling), they can be switched between an amorphous (glassy) and a crystalline state.

2.2.7 Metallic glass: Metallic glasses (sometimes also referred to as glassy metals or, inappropriately, as amorphous metals) are non-crystalline materials composed of either pure metals or combinations of metals and materials. Metallic glasses also have an incredible ability to store and release elastic energy, which makes them perfect for sports equipment, like tennis racquets, golf clubs, and skis. They're resistant to corrosion, and can be cast into complex shapes with mirror-like surfaces in a single moulding step.

2.3 Types of glass base on their application: -

2.3.1 Water glass: It is made by heating a mixture of sodium carbonate and silica to form a mixture of sodium silicate. It is water-soluble.

2.3.2 Photochromic Glass: This is a specific type of glass that turns black when exposed to bright light, making it ideal for use as a light protector and eye reliever on eye

lenses and goggles. The main reason for the blackening of the glasses is the presence of silver iodide.

2.3.3 Pyrex glass: Borosilicate glass is another name for this. It has many special chemical properties as well as high heat content in sensitive resistivity.

2.3.4 Lead Crystal Glass: This is a unique glass that can be used to create a wide variety of beautiful objects using appropriate decorative, cutting and designing techniques. In fact, when such glasses are shattered, the optical phenomenon of overall interior reflection occurs very intensely, resulting in a pleasant bright light.

2.3.5 Soda glass: Soda glass also known as soft glass, it is the cheapest and most widely used type of glass. It is easily damaged and cracks can form in such mirrors as a result of temperature changes.

2.3.6 Xena Glass: It is the most advanced type of glass, and is used to make chemical containers and scientific equipment. This glass is made mostly of zinc and barium borosilicate, resulting in a soft and high-quality product.

2.3.7 Flint glass: It is made of sodium, potassium and lead silicates, which are used to make culturally important statues, as well as expensive glassware and technologies. These mirrors are made of electric lights,

telescopes, microscopes, cameras and prism lenses, among other things.

2.3.8 Crown glass: This is usually soda-lime silica glass, commonly used in the manufacture of spectacle lenses.

2.3.9 Crooks Glass: Cerium oxide is the main component of this glass, which effectively absorbs UV wavelengths from sunlight and is used to make spectacle lenses.

CHAPTER 3

METHODS OF GLASS PREPARATION

Several techniques are available for the preparation of glasses. Some of these are listed below –

1. Melt quenching
2. Electrolytic deposition
3. Chemical reaction
4. Glow- discharge decomposition
5. Thermal evaporation
6. Shockwave transformation
7. Sol – gel method
8. Sputtering

3.1 Melt Quenching Method

The glass specimen will be prepared by melt quenching technique using muffle furnace. The weighted quantities of constituents of the desired glass are ground for 2 hours in an automatic agate mortar to attain the homogeneity. These batch materials are then heated in an alumina crucible to 1000˚ C. the working temperature is maintained for 6 hours to ensure the melt to be from gases. The melt is shaken several times to ensure homogeneity. The melt is quickly transferred in heavy copper moulds and allowed to cool for 24 hours. The glass specimens so prepared are annealed for 4 hours at about 300˚

C to remove the strains. The specimens are than cut and polished with cerium oxide and again annealed to remove strains and fatigue.

The prepared samples will be characterized by XRD. The physical parameters like densities of specimens will be measured by displacement method using high purity A.R. grade benzene and sensitive single pan balance. The refractive indices of glass specimen will be determined using Abbe refractometer. The absorption and fluorescence spectra in range 220 – 800 nm will be measured.

3.2 Electrolysis Deposition

We have heard of the coating of one metal on another metal using the process of electrolysis. We have also heard about copper plating and silver plating in our daily lives. In this article, let us discuss in brief electrolysis and electroplating along with their applications.

What is electrolyte?

The word “electrolysis” was introduced by Michael Faraday in the 19th century. In chemistry, electrolysis is a method that uses a direct current (DC) to drive a non-spontaneous chemical reaction. This technique is commercially significant as a stage in the separation of elements from naturally occurring sources such as ores using an electrolytic cell.

Electrolysis Process

The fundamental process of electrolysis is the interchanging of ions and atoms by the addition or removal of electrons from the external circuit.

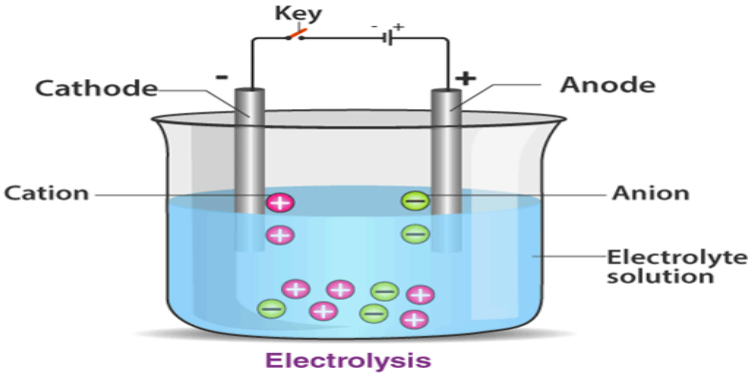

1. Ionic compounds contain charged particles called ions. For example, sodium chloride contains positively charged sodium ions and negatively charged chlorine ions.
2. The ions must be free to move in order to start the electrolysis process. When an ionic substance is dissolved in water or melted then the ions are free to move. During electrolysis, positively charged ions move to the negative electrode and negatively charged ions move to the positive electrode. Then positively charged ions receive electrons and negatively charged ions lose electrons. Both the products of the dissociation get collected at the electrodes.
3. For instance, if electricity is passed through molten sodium chloride, the sodium chloride is broken into

sodium and chlorine, and they collect at their respective electrodes. The metals get precipitated and the gases escape. This ability to break down a substance with a current is used in many ways.

4. Electrolysis is widely used for electroplating.

Why Is Aluminium No Longer a Precious Metal?

In medieval times, aluminium was almost as precious as silver. Its extraction was not known and pure aluminium was extremely hard to come by. The application of electrolysis turned aluminium from a precious metal to one of the most largely used metals by humans. Aluminium is extracted from its ore by the process of electrolytic decomposition and deposition.

Uses of Electrolysis

1. Coating one metal on another.
2. The industrial use includes various metals such as aluminium, magnesium, chlorine, and fluorine etc.

3.3 Chemical reaction

The process of chemical reactions between components in the production of a glass-forming melt in the Na_2O – SiO_2 system is considered taking into account the surface and volumetric factors. The kinetic analysis of the process is implemented and a mechanism of interaction of Na_2CO_3 melt with solid SiO_2 is proposed.

3.4 Glow- discharge decomposition

A glow discharge is initiated under Ar atmosphere with the sample as cathode. When Ar atoms collide with the

sample, its constituent elements are sputtered. Most of the sputtered elements are neutral but they are ionized by the Ar plasma.

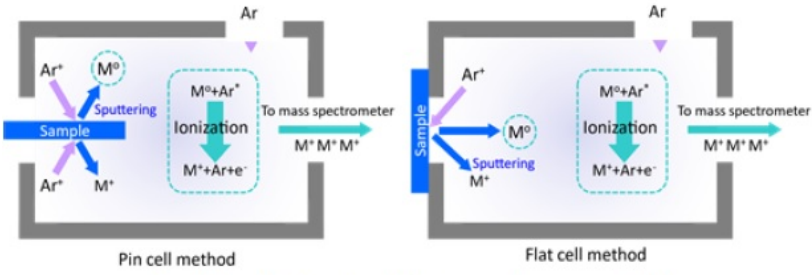

3.5 Thermal evaporation

Thermal evaporation is a well-known method for coating a thin layer in which the source material evaporates in a vacuum due to high temperature heating, which facilitates the vapour particles moving and directly reaching a substrate where these vapours again change to a solid state.

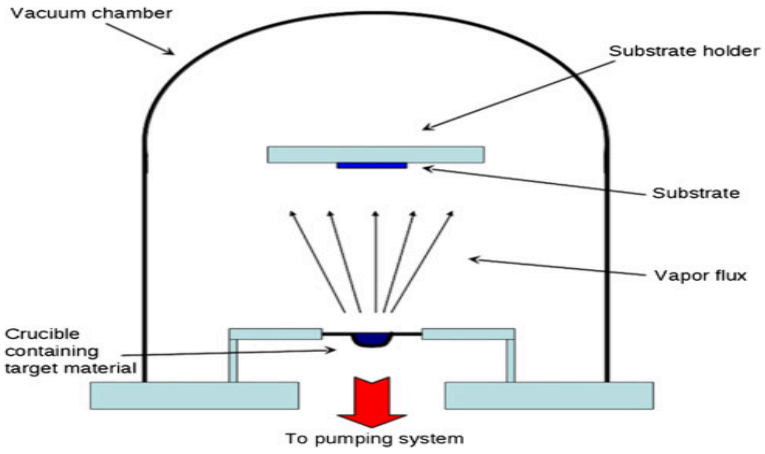

3.6 Shockwave transformation

Shock wave causes rapid fusing of the powders without the melt and subsequent grain growth of other techniques, which describe the test setup and consolidation results.

3.7 Sol- gel method

Sol–gel processing of a bulk glass consists of processes of wet gel formation, drying of the gel, and subsequent sintering of the gel to glass by heating. Among these processes, drying of a wet gel body is one of the critical processes when one desires to make a bulk glass without cracks and fracture.

3.8 Sputtering

Sputter deposition is a widely used physical vapor deposition method and has advantages over techniques such as pulsed laser or molecular beam epitaxy when it comes to making large-area films for numerous industrial applications. Perhaps because of this common emphasis on quickly producing large-area films, however, sputter deposition does not necessarily broadly enjoy the reputation it deserves for producing high-quality epitaxial films of complex oxides for research purposes. The truth is that high-quality epitaxial thin films and super lattices of complex oxides can indeed be achieved using sputter deposition, often at a significantly lower cost than other techniques. With each wave of interest in a particular class of complex oxide materials, a route to high-quality oxide films through sputtering has usually been found, and the resulting films have been important enablers of scientific progress.

CHAPTER 4

CHARACTERIZATION TECHNIQUES

Introduction

Characterization techniques used in material science, refers to the broad and general process why which a material's structure and properties are probed in measured these are fundamental processes in the field of material science without which no scientific understanding. Several characterization techniques are using for charactering different properties of glass and rare earth ions doped glasses as given below-

4.1 X-ray diffraction

X-ray diffraction (XRD) is a non-destructive technique for analyzing the structure of materials, primarily at the atomic or molecular level. It works best for materials that are crystalline or partially crystalline but is also used to study non-crystalline materials.

XRD relies on the fact that X-rays are a form of light, with wavelengths on the order of nanometres. When X-rays scatter from a substance with structure at that length scale, interface can take place, resulting in a pattern of higher and lower intensities. This is qualitatively similar to the colourful patterns produced by soap bubbles, in which different colors are viewed in different directions.

XRD is quite different from X-ray radiography or tomography. Tomography relies on the fact that the X-rays are absorbed more strongly by some materials than others--for example, bone or tumours absorb more than muscle or fat. Therefore, the transmitted image provides a direct image of the structure inside the body or object making it an invaluable tool for doctors. In contrast, the XRD produces a diffraction pattern, which does not superficially resemble the underlying structure, and provides information about the internal structure on length scales from 0.1 to 100 nm.

In its most simplified form, a generic X-ray scattering measurement is shown below.

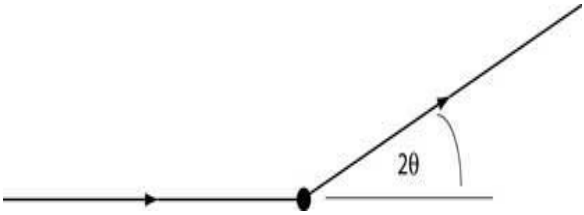

A beam of X- rays is directed towards a sample, and the scattered intensity is measured as a function of outgoing direction. By convention, the angle between the incoming and outgoing beam directions is called 2θ. For the simplest possible sample, consisting of sheets of charge separated by a distance *d, constructive interference (greater scattered intensity) is observed when Bragg's Law is satisfied*

$$n\lambda = 2\,d \sin\theta$$

Here *n* is an integer (1, 2, 3....), λ is the wavelength of the x- ray beam, and θ is half the scattering angle 2θ shown above.

Real materials are more complicated, of course, but the general result holds that there is a relationship between interparticle distances within the sample and the angles at which the scattered intensity is the highest, with larger distances *d* corresponding to smaller scattering angles 2θ.

What are the components of an x-ray diffraction instrument?

Although there are many possible permutations, essentially all XRD instruments incorporate the components shown in the following schematic: a means of producing the x-ray radiation, some kind of collimation, something to support the sample (and possibly orient it or maintain a desired environment), and a means for detecting the scattered radiation.

Production of X-rays:

There are a variety of methods for producing a beam of x-rays.

X-ray Tube:

This is the simplest and oldest approach, and is still occasionally used. A beam of electrons strikes a metallic target and X-rays are emitted. The intensity of the X-ray beam is limited by the heat released into the target by the electron beam.

Rotating anode X-ray generator:

This variant of the traditional X-ray tube, which became widely available in the 1970's, addresses the heat loading problem by replacing the fixed target with a rotating cylinder, water-cooled on the inside. Considerably more X-ray intensity is thereby made possible, but there are both literal and figurative costs: the engineering requirements are considerably more stringent, and rotating-anode generators are subject to breakdowns and require frequent maintenance.

Microfocus Tube:

The most recent solution to the heat loading problem takes a different tack: the electron beam is focused down to a tiny spot (typically 50 μm or less in diameter), so that the total heat load on the anode is quite small. Micro source tubes started to become available around 2000, and are gradually replacing rotating anode generators.

Synchrotron:

A synchrotron X-ray source uses a totally different mechanism from the tube sources described above: the radiation emitted from a relativistic beam of electrons (or positrons) accelerated by a magnetic field. The resulting beam is generally many orders of magnitude more intense than that produced by the tabletop sources described above. However, such a beam can be produced only at a large centralized facility, obliging most users to travel substantial distances and plan their usage well in advance. For this reason, tube/rotating anode/micro focus sources, which can be operated at the user's home institution, are best suited for relatively routine measurements, while synchrotron sources are required for experiments requiring extremely high intensity or other specialized conditions.

Collimation:

The radiation produced by any of the above mechanisms consists in general of rays traveling in a variety of directions and consisting of a spread of wavelengths. The purpose of the collimation portion of an XRD instrument is to produce a relatively thin beam of X-rays with a narrow spread of wavelengths, all traveling in essentially the same direction. Some commonly used components are described below.

Slits or pinholes:

These form a part of almost every instrument, and act by geometrically restricting the beam. To be effective, they must be constructed from a heavy element such as tungsten.

Care must be taken to minimize diffuse ("parasitic") scattering from the edges of the slits which can contribute to the background signal.

Crystal Monochromatic:

The most common method for producing a "monochromatic" beam (containing only a narrow spread of wavelengths λ) is to insert a high-quality single crystal of a material such as silicon or germanium into the beam and separate out only those components of the beam that satisfy Bragg's Law. Conversely, for a beam that is already largely monochromatic, this Bragg reflection from a crystal can be used as a means of collimation. The degree of collimation and spectral selection depend on the perfection of the crystal and also the characteristics of the incoming beam.

***X-ray Mirror*:**

X-ray mirrors rely on the same effect referred to in our discussion of X-ray reflectivity, namely that a beam which strikes a flat surface at a very low angle can be strongly reflected. X-ray mirrors are typically made of a metal such as gold and are gently curved so as to produce a beam that is focused along a vertical and/or horizontal axis. They also affect the spectral characteristics since shorter wavelengths are reflected much less effectively than long wavelengths.

***Multilayer Optics*:**

This approach, which is incorporated in many units currently on the market (especially those optimized for small-angle scattering) combines the benefits of a crystal

monochromatic and an X-ray mirror. A multilayer coating on a curved substrate results in a monochromatic, collimated beam, most often either parallel or slightly convergent focus. The optical unit must be closely coupled with the source, but when done properly this can result in a beam that is simultaneously more intense and better collimated than achievable with previous technologies.

Sample Support:

Clearly, the sample must be placed in the centre of the beam. The exact means for achieving this depends on the nature of the sample, which is quite often a small single crystal, a solid slab, a powder, a thin film supported on a substrate, or a liquid. If the sample is a powder or a liquid, it is enough to place the sample in the beam. If single-crystal measurements are performed, the orientation of the sample is also crucial, and is set and varied by mounting the sample on a monometer. Most measurements are made at room temperature, under ambient conditions. However, specialized instruments may control the temperature of the sample, apply a magnetic field, shear the sample, etc.

Detection:

The last stage in any XRD instrument must be some means of detecting the scattered X-rays. A rough historical progression of X-ray detection technologies follows:

Film:

For most of the 20th century photographic plates or films, generally coupled with some kind of X-ray fluorescent

screen, were the dominant method for measuring diffraction patterns. A collimated beam struck the sample, and then the plate was placed behind the sample. This method was easy to deploy, but it was difficult to convert the images to quantitative plots. Photographic plates are still often used in medical X-ray radiography.

Scintillation Detector:

Starting around the 1970's, film was largely replaced by solid state detectors, especially scintillation detectors that produced an electronic readout of the scattered intensity that could be directly read by a computer. Because scintillation detectors generally measure the scattered intensity at only one angle at a time, some type of collimation is necessary between the sample and the detector, often similar to that found between the source and the detector. Systems employing "point detector" are thus intrinsically somewhat slow, because only one angle is measured at a time, but are usually an improvement over photographic film due to their high sensitivity and easy readout in digital form.

***2D Detector*:**

Two-dimensional, or "area" detectors came into increasing use around 1990. A number of different technologies are available, but all of them function essentially as "electronic film": like photographic film, they record the intensity across an entire surface, but the resultant image is directly transmitted to the data-taking computer as an array of intensities. In most cases, the intensity report for each pixel is

an integer quantity, and is equal or at least proportional to the number of X-ray photons that struck that pixel in a certain amount of time. Area detectors combine many of the advantages of scintillation detectors and film. They are highly sensitive, and can be read out rapidly, but measure the diffraction at many angles simultaneously. The volume of data produced is thus greatly increased; a single data frame from an area detector generally occupies at least 1Mb of disk space, and often 10 Mb or more.**UV-VIS Spectrometer**

4.2 What is UV-Vis spectroscopy?

UV-Vis spectroscopy is an analytical technique that measures the number of discrete wavelengths of UV or visible light that are absorbed by or transmitted through a sample in comparison to a reference or blank sample. This property is influenced by the sample composition, potentially providing information on what is in the sample and at what concentration. Since this spectroscopy technique relies on the use of light, let's first consider the properties of light.

Light has a certain amount of energy which is inversely proportional to its wavelength. Thus, shorter wavelengths of light carry more energy and longer wavelengths carry less energy. A specific amount of energy is needed to promote electrons in a substance to a higher energy state which we can detect as absorption. Electrons in different bonding environments in a substance require a different specific amount of energy to promote the electrons to a higher energy state. This is why the absorption of light occurs for different

wavelengths in different substances. Humans are able to see a spectrum of visible light, from approximately 380 nm, which we see as violet, to 780 nm, which we see as red. UV light has wavelengths shorter than that of visible light to approximately 100 nm. Therefore, light can be described by its wavelength, which can be useful in UV-Vis spectroscopy to analyse or identify different substances by locating the specific wavelengths corresponding to maximum absorbance.

How does a UV-Vis spectrophotometer work?

Whilst there are many variations on the UV-Vis spectrophotometer, to gain a better understanding of how an UV-Vis spectrophotometer works, let us consider the main components, depicted in Figure 4.2.1.

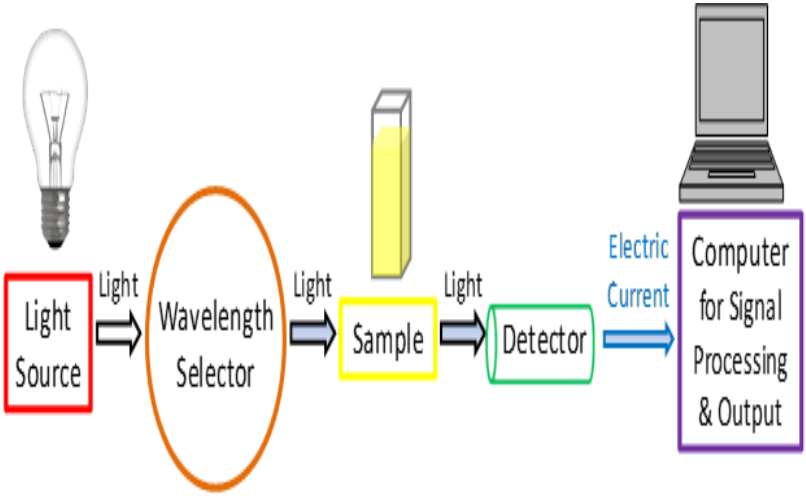

Figure 4.2.1: A simplified schematic of the main components in a UV-Vis spectrophotometer

Light source:

As a light-based technique, a steady source able to emit light across a wide range of wavelengths is essential. A single xenon lamp is commonly used as a high intensity light source for both UV and visible ranges. Xenon lamps are, however, associated with higher costs and are less stable in comparison to tungsten and halogen lamps.

For instruments employing two lamps, a tungsten or halogen lamp is commonly used for visible light, whilst a deuterium lamp is the common source of UV light. As two different light sources are needed to scan both the UV and visible wavelengths, the light source in the instrument must switch during measurement. In practice, this switchover typically occurs during the scan between 300 and 350 nm where the light emission is similar from both light sources and the transition can be made more smoothly.

Wavelength selection:

In the next step, certain wavelengths of light suited to the sample type and analyte for detection must be selected for sample examination from the broad wavelengths emitted by the light source. Available methods for this include:

1. **Monochromators:**

A monochromatic separates light into a narrow band of wavelengths. It is most often based on diffraction gratings that can be rotated to choose incoming and reflected angles to select the desired wavelength of light. The diffraction grating's groove frequency is often measured as the number of grooves per mm. A higher groove frequency provides a better

optical resolution but a narrower usable wavelength range. A lower groove frequency provides a larger usable wavelength range but a worse optical resolution. 300 to 2000 grooves per mm is usable for UV-Vis spectroscopy purposes but a minimum of 1200 grooves per mm is typical. The quality of the spectroscopic measurements is sensitive to physical imperfections in the diffraction grating and in the optical setup.

2. **Absorption filters:**

Absorption filters are commonly made of colored glass or plastic designed to absorb particular wavelengths of light.

3. **Interference filters**:

Also called dichroic filters, these commonly used filters are made of many layers of dielectric material where interference occurs between the thin layers of materials. These filters can be used to eliminate undesirable wavelengths by destructive interference, thus acting as a wavelength selector.

4. **Cut-off filters:**

Cut-off filters allow light either below (short pass) or above (long pass) a certain wavelength to pass through. These are commonly implemented using interference filters.

5. **Bandpass filters:**

Bandpass filters allow a range of wavelengths to pass through that can be implemented by combining short pass and long pass filters together. Monochromators are most commonly used for this process due to their versatility.

However, filters are often used together with monochromators to narrow the wavelengths of light selected further for more precise measurements and to improve the signal-to-noise ratio.by the instrument to help obtain the true absorbance values of the analytes.

Detection:

After the light has passed through the sample, a detector is used to convert the light into a readable electronic signal. Generally, detectors are based on photoelectric coatings or semiconductors.

A **photoelectric coating** ejects negatively charged electrons when exposed to light. When electrons are ejected, an electric current proportional to the light intensity is generated. A photomultiplier tube (PMT) is one of the more common detectors used in UV-Vis spectroscopy. A PMT is based on the photoelectric effect to initially eject electrons upon exposure to light, followed by sequential multiplication of the ejected electrons to generate a larger electric current. PMT detectors are especially useful for detecting very low levels of light. When **semiconductors** are exposed to light, an electric current proportional to the light intensity can pass through. More specifically, photodiodes and charge-coupled devices (CCDs) are two of the most common detectors based on semiconductor technology. After the electric current is generated from whichever detector was used, the signal is then recognized and output to a computer or screen. Figures 4.2.2 and 4.2.3 show some simplified example schematic diagrams of UV-Vis spectrophotometer arrangements.

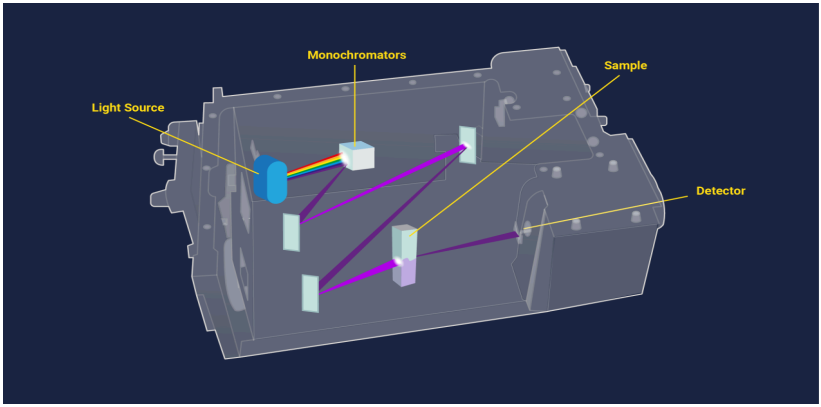

Figure 4.2.2: Schematic diagram of a cuvette-based UV-Vis spectroscopy system.

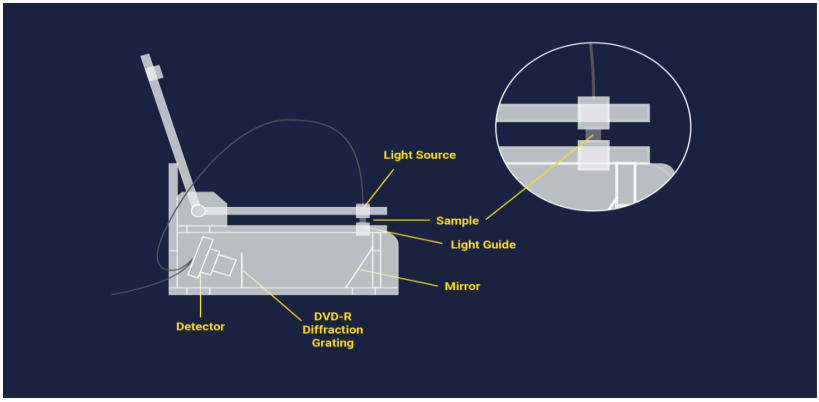

Figure 4.2.3: Schematic diagram of a cuvette-free UV-Vis spectroscopy system.

UV-Vis spectroscopy information may be presented as a graph of absorbance, optical density or transmittance as a function of wavelength. However, the information is more often presented as a graph of absorbance on the vertical *y* axis and wavelength on the horizontal *x* axis. This graph is typically

referred to as an absorption spectrum; an example is shown in Figure 4.2.4.

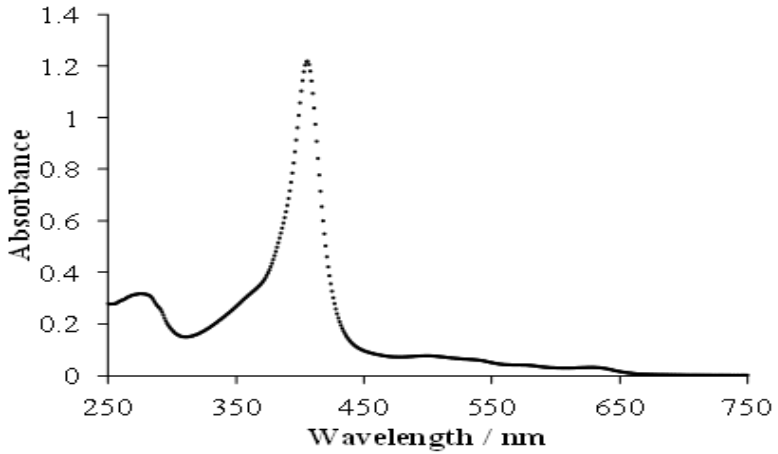

Figure 4.2.4: An example absorption spectrum taken from a UV-Vis spectrophotometer. The sample examined was expired hemoglobin dissolved in neutral pH phosphate buffer.

Based on the UV-Vis spectrophotometer instrumentation reviewed in the previous section of this article, the intensity of light can be reasonably expected to be quantitatively related to the amount of light absorbed by the sample. The absorbance (A) is equal to the logarithm of a fraction involving the intensity of light before passing through the sample (I_o) divided by the intensity of light after passing through the sample (I). The fraction I divided by I_o is also called transmittance (T), which expresses how much light has passed through a sample. However, Beer–Lambert's law is often applied to obtain the concentration of the sample (c) after

measuring the absorbance (A) when the molar absorptivity (ε) and the path length (L) are known. Typically, ε is expressed with units of L mol^{-1} cm^{-1}, L has units of cm, and c is expressed with units of mol L^{-1}. As a consequence, A has no units. Sometimes AU is used to indicate arbitrary units or absorbance units but this has been strongly discouraged. Beer–Lambert's law is especially useful for obtaining the concentration of a substance if a linear relationship exists using a measured set of standard solutions containing the same substance. Equation 1 shows the mathematical relationships between absorbance, Beer–Lambert's law, the light intensities measured in the instrument, and transmittance.

$$A = \varepsilon Lc = log_{10}\left(\frac{I_0}{I}\right) = log_{10}\left(\frac{1}{T}\right) = - log_{10}(T) \quad \text{..... (1)}$$

A set of equations showing the relationships between absorbance A, Beer–Lambert's law, the light intensities measured in the instrument, and transmittance. The term optical density (OD) is sometimes incorrectly used interchangeably with absorbance. OD and absorbance both measure the amount of light intensity lost in an optical component, but OD takes into consideration loss from light scattering whereas absorbance does not. If very little light scattering is present in a measurement, then OD may be approximated directly using absorbance and Beer–Lambert's law may be used. Knowing the experimental conditions during measurements is important. Cuvettes designed for a 1 cm path length are standard and are most common. Sometimes, very

little sample is available for examination and shorter path lengths as small as 1 mm are necessary. Where quantitation is required, absorbance values should be kept below 1, within the dynamic range of the instrument. This is because an absorbance of 1 implies that the sample absorbed 90% of the incoming light, or equivalently stated as 10% of the incoming light was transmitted through the sample. With such little light reaching the detector, some UV-Vis spectrophotometers are not sensitive enough to quantify small amounts of light reliably. Two simple possible solutions to this problem are to either dilute the sample or decrease the path length.

As mentioned above, recording a baseline spectrum using a "blank" reference solution is essential. If the instrument was absolutely perfect in every way, the baseline would have zero absorbance for every wavelength examined. In a real situation, however, the baseline spectrum will usually have some very small positive and negative absorbance values. For best practice, these small absorbance values are often automatically subtracted from the sample absorbance values for each wavelength of light by the software to obtain the true absorbance values.

Depending on the purpose of the analysis, the construction of a calibration curve may be desirable. Building a calibration curve requires some data analysis and extra work but it is very useful to determine the concentration of a particular substance accurately in a sample based on absorbance measurements. There are however, numerous circumstances in which a calibration curve is not necessary

including OD measurements for bacterial culturing, taking absorbance ratios at specific wavelengths for assessing the purity of nucleic acids or identifying certain pharmaceuticals.

In UV-Vis spectroscopy, the wavelength corresponding to the maximum absorbance of the target substance is chosen for analysis. This choice ensures maximum sensitivity because the largest response is obtained for a certain analyte concentration. An example of a UV Vis absorption spectrum of Food Green 3 and a corresponding calibration curve using standard solutions are provided in Figure 5. Note that two maximum absorbance peaks are present in the Food Green 3 dye, a smaller maximum absorbance peak at 435 nm and a more intense maximum absorbance peak at 619 nm. To gain maximum sensitivity when calculating an unknown concentration of Food Green 3, the maximum absorbance peak at 619 nm was used for analysis. Standard solutions across a range of known concentrations were prepared by diluting a stock solution, taking absorbance measurements and then plotting these on a graph of absorbance versus concentration to build a numerical relation between concentration and absorbance. A calibration curve was created using a least squares linear regression equation. The closer the data points are to a straight line, the better the fit. The y intercept in the straight-line equation was set to zero to indicate no absorbance when no dye was present. The equation shown in Figure 4.2.5 is used to calculate the concentration of Food Green 3 (variable x) in an unknown sample based on the measured absorbance (variable y).

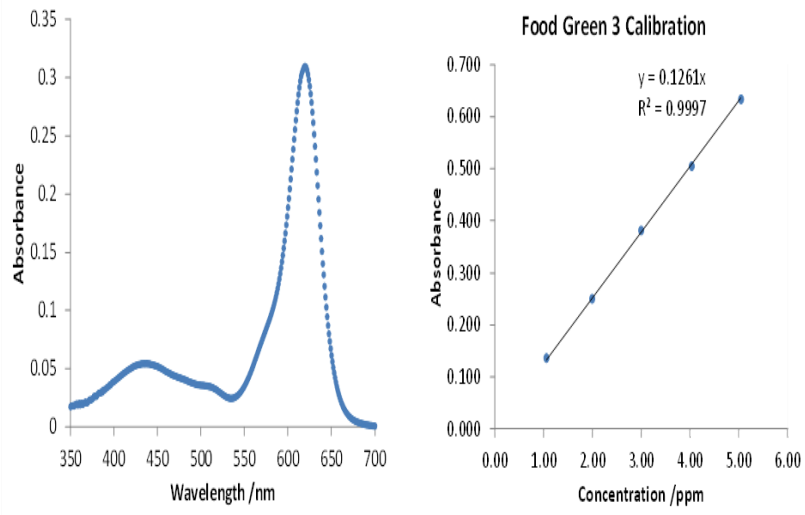

Figure 4.2.5:

A UV-Vis spectrum of Food Green 3 extracted from a sample is shown on the left graph. A calibration curve shown on the right graph was developed from standard diluted solutions of Food Green 3 using a least squares linear regression equation.

For data analysis, the graph of absorbance versus concentration can indicate how sensitive the system is when building a calibration curve. When a linear least squares regression equation is used, the slope from the line of best fit indicates sensitivity. If the slope is steeper, the sensitivity is higher. Sensitivity is the ability to differentiate between the small differences in the sample concentration. From Beer–Lambert's Law, the sensitivity can be partially indicated by the molar absorptivity ε. knowing the ε values beforehand,

if available, can help to determine the concentrations of the samples required, particularly where samples are limited or expensive.

For reliability and best practice, UV-Vis spectroscopy experiments and readings should be repeated. When repeating the examination of a sample, in general, a minimum of three replicate trials is common, but many more replicates are required in certain fields of work. A calculated quantity, such as the concentration of an unknown sample, is usually reported as an average with a standard deviation. Reproducible results are essential to ensure precise, high-quality measurements. Standard deviation, relative standard deviation, or the coefficient of variation help to determine how precise the system and measurements are. A low deviation or variation indicates a higher level of precision and reliability.

Strengths and limitations of UV-Vis spectroscopy

No single technique is perfect and UV-Vis spectroscopy is no exception. The technique does, however, have a few main **strengths** listed below that make it popular.

1. The technique is **non-destructive**, allowing the sample to be reused or proceed to further processing or analyses.
2. Measurements can be made **quickly**, allowing easy integration into experimental protocols.
3. Instruments are **easy to use**, requiring little user training prior to use.
4. Data analysis generally requires **minimal processing**, again meaning little user training is required.

5. The instrument is generally **inexpensive** to acquire and operate, making it accessible for many laboratories.

Although the strengths of this technique seem overwhelming, there are also certain **weaknesses**

1. **Stray light:**

   In a real instrument, wavelength selectors are not perfect and a small amount of light from a wide wavelength range may still be transmitted from the light source, possibly causing serious measurement errors. Stray light may also come from the environment or a loosely fitted compartment in the instrument.

2. **Light scattering:**

   Light scattering is often caused by suspended solids in liquid samples, which may cause serious measurement errors. The presence of bubbles in the cuvette or sample will scatter light, resulting in irreproducible results.

3. **Interference from multiple absorbing species:**

   A sample may, for example, have multiple types of the green pigment chlorophyll. The different chlorophylls will have overlapping spectra when examined together in the same sample. For a proper quantitative analysis, each chemical species should be separated from the sample and examined individually.

4. **Geometrical considerations:**

   Misaligned positioning of any one of the instrument's components, especially the cuvette holding the sample, may yield irreproducible and inaccurate results. Therefore, it is important that every component in the instrument is aligned

in the same orientation and is placed in the same position for every measurement. Some basic user training is therefore generally recommended to avoid misuse.

4.3 Ramanand Surface-Enhanced Raman Spectroscopy

What is Raman Spectroscopy?

Raman spectroscopy is a powerful tool for determining chemical species. As with other spectroscopic techniques, Raman spectroscopy detects certain interactions of light with matter. In particular, this technique exploits the existence of Stokes and Anti-Stokes scattering to examine molecular structure. When radiation in the near infrared (NIR) or visible range interacts with a molecule, several types of scattering can occur. Three of these can be seen in the energy diagram in Figure 4.3.1.

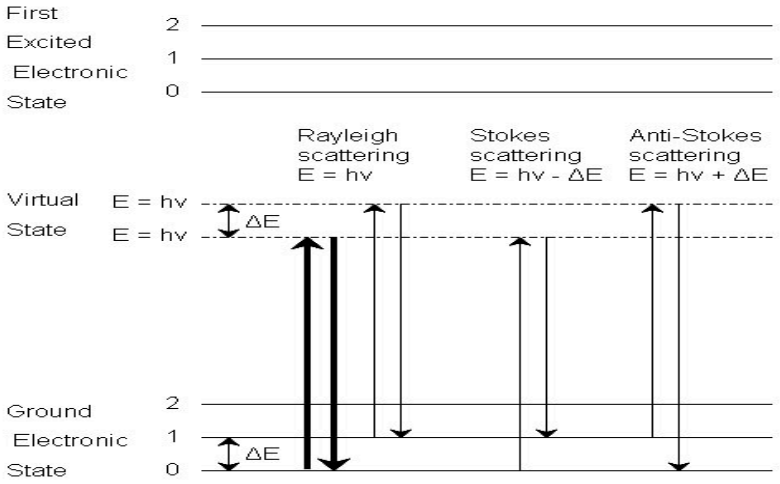

Figure 4.3.1: **Three types of scattering by a molecule excited by a photon with energy E = hv.**

The most common transition is marked with bold arrows. In all three types of scattering, an incident photon of energy hν raises the molecule from a vibrational state to one of the infinite numbers of virtual states located between the ground and first electronic states. The type of scattering observed is dependent on how the molecule relaxes after excitation.

Rayleigh Scattering

1. The molecule is excited to any virtual state.
2. The molecule relaxes back to its original state.
3. The photon is scattered elastically, leaving with its original energy.

Stokes Scattering

1. The molecule is excited to any virtual state.
2. The molecule relaxes back to a higher vibrational state than it had originally.
3. The photon leaves with energy hν-ΔE and has been scattered inelastically.

Anti-Stokes Scattering

1. The molecule begins in a vibrationally excited state.
2. The molecule is excited to any virtual state.
3. The molecule relaxes back to a lower vibrational state than it had originally.

The photon leaves with energy hν+ΔE, and has been scattered super elastically.Rayleigh scattering is by far the most common transition, due to the fact that no change has to occur in the vibrational state of the molecule. The anti-Stokes

transition is the least common, as it requires the molecule to be in a vibrationally excited state before the photon is incident upon it. Due to the lack of intensity of the anti-Stokes signal and filtering requirements that eliminate photons with incident energy and higher, generally only Stokes scattering is used in Figure 4.3.2

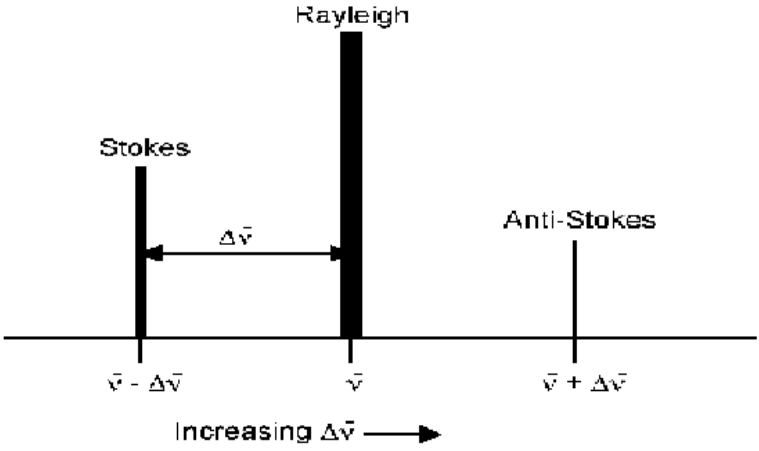

Figure 4.3.2: Location and relative intensity (indicated by peak height and width) of the Stokes and anti-Stokes scattering relative to Rayleigh scattering.

Raman spectroscopy observes the change in energy between the incident and scattered photons associated with the Stokes and anti-Stokes transi tions. This is typically measured as the change in the wave number (cm^{-1}), from the incident light source. Because Raman measures the change in wave number, measurements can be taken using a source at any

wavelength; however, near infrared and visible radiation are commonly used. Photons with ultraviolet wavelengths could work as well, but tend to cause photodecomposition of the sample.

Comparison between Raman and Infrared Spectroscopy

Raman spectroscopy sounds very much like infrared (IR) spectroscopy; however, IR examines the wavenumber at which a functional group has a vibrational mode, while Raman observes the shift in vibration from an incident source. The Raman frequency shift is identical to the IR peak frequency for a given molecule or functional group. As mentioned above, this shift is independent of the excitation wavelength, giving versatility to the design and applicability of Raman instruments.

The cause of the vibration is also mechanistically different between IR and Raman. This is because the two operate on different sets of selection rules. IR absorption requires a dipole moment or change in charge distribution to be associated with the vibrational mode. Only then can photons of the same energy as the vibrational state of molecule interact.

What does Raman Spectroscopy Measure?

Raman activity depends on the polarizability of a bond. This is a measure of the deformability of a bond in an electric field. This factor essentially depends on how easy it is for the electrons in the bond to be displaced, inducing a temporary dipole. When there is a large concentration of loosely held

electrons in a bond, the polarizability is also large, and the group or molecule will have an intense Raman signal. Because of this, Raman is typically more sensitive to the molecular framework of a molecule rather than a specific functional group as in IR. This should not be confused with the polarity of a molecule, which is a measure of the separation of electric charge within a molecule. Polar molecules often have very weak Raman signals due to the fact that electronegative atoms hold electrons so closely.

Raman spectroscopy can provide information about both inorganic and organic chemical species. Many electron atoms, such as metals in coordination compounds, tend to have many loosely bound electrons, and therefore tend to be Raman active. Raman can provide information on the metal ligand bond, leading to knowledge of the composition, structure, and stability of these complexes. This can be particularly useful in metal compounds that have low vibrational absorption frequencies in the IR. Raman is also very useful for determining functional groups and fingerprints of organic molecules. Often, Raman vibrations are highly characteristic to a specific molecule, due to vibrations of a molecule as a whole, not in localized groups. The groups that do appear in Raman spectra have vibrations that are largely localized within the group, and often have multiple bonds involved.

Sample Preparation and Instrumental Details

The standard Raman instrument is composed of three major components. First, the instrument must have an

illumination system. This is usually composed of one or more lasers. The major restriction for the illumination system is that the incident frequency of light must not be absorbed by the sample or solvent. The next major component is the sample illumination system. This can vary widely based on the specifics of the instrument, including whether the system is a standard macro-Raman or has micro-Raman capabilities. The sample illumination system will determine the phase of material under investigation. The final necessary piece of a Raman system is the spectrometer. This is usually placed 90° away from the incident illumination and may include a series of filters or a monochromator. An example of a macro-Raman and micro-Raman setup can be Figure 4.3.3 And Figure 4.3.4 A macro-Raman spectrometer has a spatial resolution anywhere from 100 μm to one millimetre while a micro-Raman spectrometer uses a microscope to magnify its spatial resolution

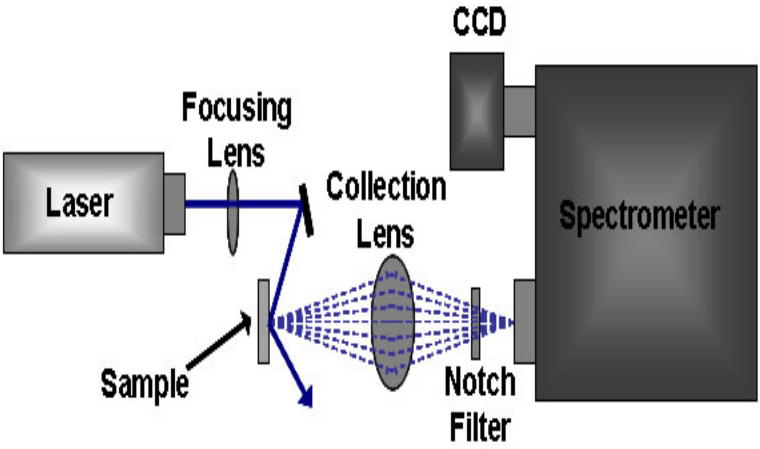

Figure 4.3.3: Schematic of a macro-Raman spectrometer.

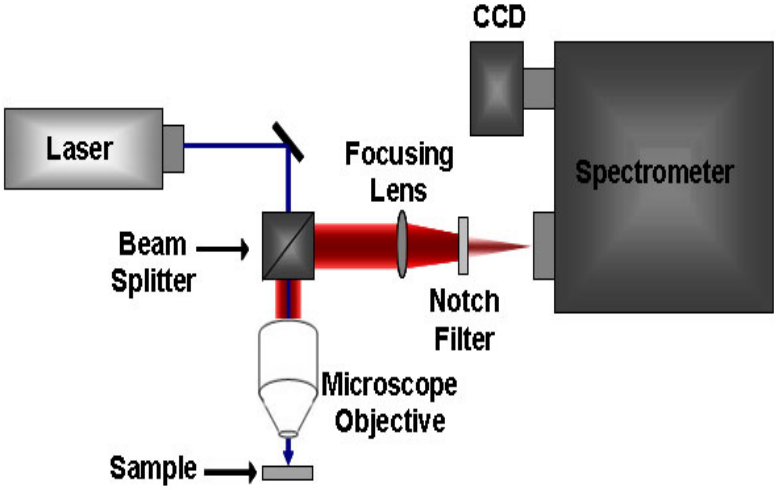

Figure 4.3.4: Schematic of a micro-Raman spectrometer where illumination and collection are performed through microscope objective.

4.4 Fluorescence Spectroscopy

Fluorescence is a process involving the emission of light from any substance in the excited states. Generally speaking, fluorescence is the emission of electromagnetic radiation (light) by the substance absorbed the different wavelength radiation. Its absorption and emission is illustrated in the diagram a fluorophore is excited to higher electronic and vibrational state from ground state after excitation. The excited molecules can relax to lower vibrational state due to the vibrational relaxation and, then further retune to the ground state in the form of fluorescence emissions

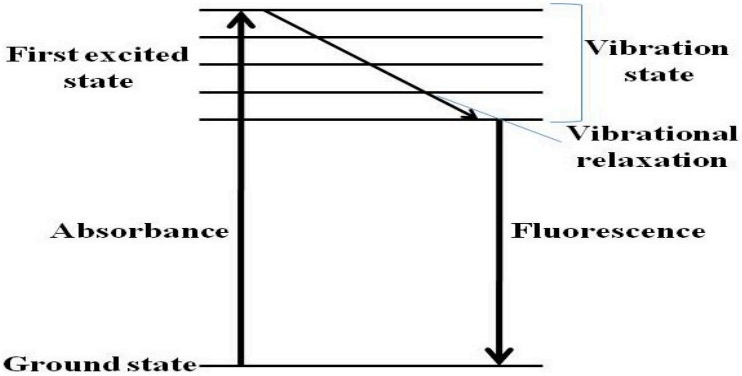

Figure 4.4.1: Energy level diagram of fluorescence spectroscopy.

Instrumentation:

Most spectrofluorometers can record both excitation and emission spectra. They mainly consist of four parts: light sources, monochromators, optical filters and detector.

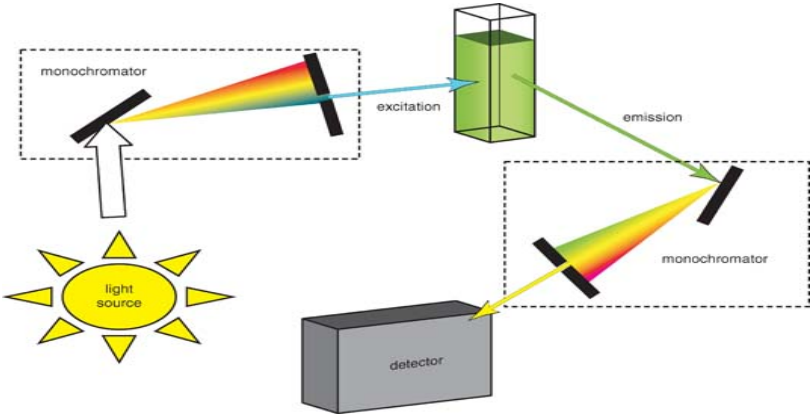

Figure 4.4.2: **Schematic representation of a fluorescence spectrometer.**

Light Sources:

Light sources that can emit wavelength of light over the ultraviolet and the visible range can provide the excitation energy. There are different light sources, including arc and incandescent xenon lamps, high-pressure mercury (Hg) lamps, Xe-Hg arc lamps, low pressure Hg and Hg-Ar lamps, pulsed xenon lamps, quartz-tungsten halogen (QTH) lamps, LED light sources, etc. The proper light source is chosen based on the application.

Monochromators:

Prisms and diffraction gratings are two mainly used types of monochromators, which help to get the experimentally needed chromatic light with a wavelength range of 10 nm. Typically, the monochromators are evaluated based on dispersion, efficiency, stray light level and resolution.

Optical Filters:

Optical filters are used in addition to monochromators in order to further purifying the light. There are two kinds of optical filters. The first one is the colored filter, which is the most traditional filter and is also divided into two categories: monochromatic filter and long-pass filter. The other one is thin film filter that is the supplement for the former one in the application and being gradually instead of coloured filter.

Detector:

An InGaAs array is the standard detector used in many spectrofluorometers. It can provide rapid and robust spectral characterization in the near-IR.

4.5 Abbé refractometer

Abbé refractometer was the first refractometer to be offered commercially its original design was so successful that even as of today it is over 154 years old, it is still used and copied in new devices. Abbé refractometer working principle is based on critical angle. Sample is put between two prisms - measuring and illuminating. Light enters sample from the illuminating prism, gets refracted at critical angle at the bottom surface of measuring prism, and then the telescope is used to measure position of the border between bright and light areas. Telescope reverts the image, so the dark area is at the bottom, even if we expect it to be in the upper part of the field of view. Knowing the angle and refractive index of the measuring prism it is not difficult to calculate refractive index of the sample. Surface of the illuminating prism is matted, so that the light enters the sample at all possible angles, including those almost

parallel to the surface. If you have seen our page on the critical angle refractometer, you already know that these rays are crucial for the working of the refractometer.

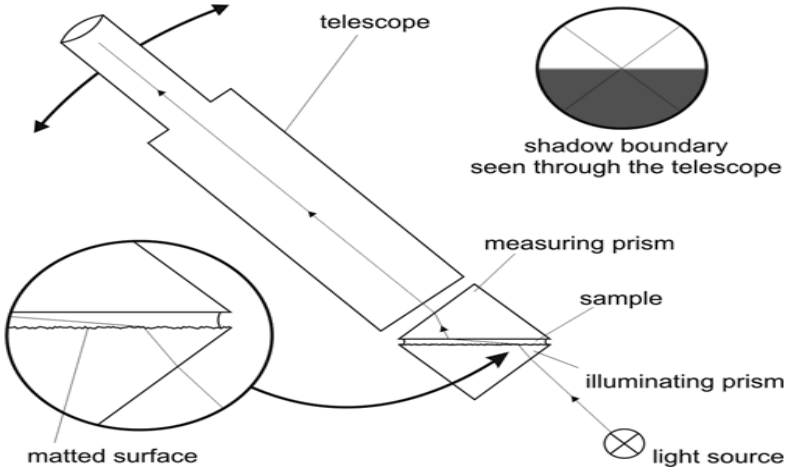

Figure 4.5.1: Block diagram of Abbe's Refractometer

While the image above already explains the basic principle, it is not yet a complete design of the Abbé refractometer. Refractive index of a substance is a function of a wavelength. If the light source is not monochromatic (and in simple devices it rarely is) light gets dispersed and shadow boundary is not well defined, instead of seeing sharp edge between white and black, you will see a blurred blue or red border. In most cases that means measurements are either very inaccurate or even impossible. To prevent dispersion Abbé added two compensating Amici prisms into his design. Not only telescope position can be changed to measure the angle, also position of Amici prisms can be adjusted, to correct the

dispersion. In effect edge of the shadow is well defined and easy to locate.

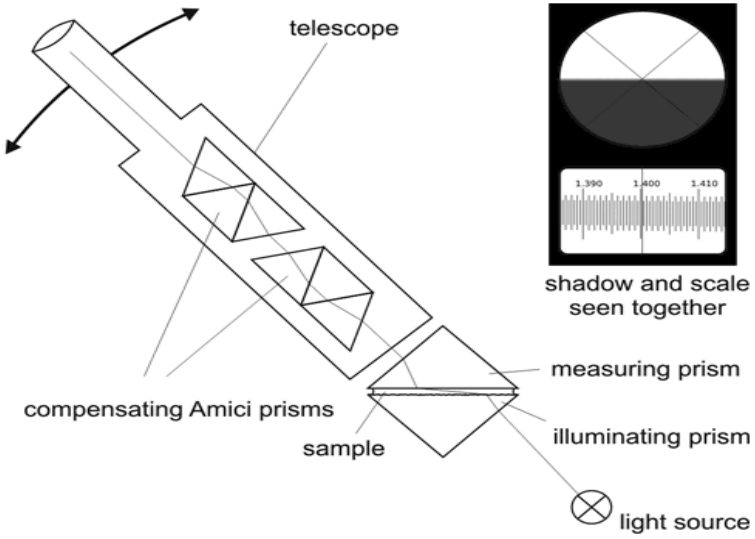

Figure 4.5.2: Abbe's Refractometer Block Diagram

Original design made use of two telescopes - one was used to locate shadow boundary, the other to read the result. Modern devices combine both views so that you can read the result immediately, without a need for checking the other view. Some specialized devices may have double scale - one can be used for reading refractive index, the other (situated below or above, and visible at the same time) can be scaled in degrees Brix or concentration of some substance.

Abbé refractometers come in many variants that differ in details of their construction. In original design whole telescope was rotated around stationary sample and scale. In

modern designs telescope position is fixed, what moves is an additional mirror between sample and telescope. Abbé refractometer can be used to measure both refractive index of liquids and solids. In both cases refractive index of the substance must be lower than the refractive index of the glass used to make measuring prism. To use the refractometer, we simply put the sample between illuminating and measuring prisms, use rotating knob to place the shadow boundary on the telescope cross hairs, and read the refractive index from the scale. Liquid samples must be non-corrosive, to not damage surface of the prisms. Abbé refractometers can give an accuracy of about one to two units in the fourth decimal place.

It is worth of noting here, that - as refractive index changes with temperature - for a correct result of refractive index measurement we have to either use thermostated sample, or - after measuring the refractive index - measure temperature and read correction from tables. Most laboratory models of Abbé refractometers are ready to be attached to the source of constant temperature water.

CHAPTER 5

INTERACTION PARAMETERS OF RE^{3+} DOPPED GLASSES

Introduction

This is essential to study the energies and intensities of the absorption bands. An attempt has been made to calculate various energy interaction parameters and bonding of rare earth ions in the several glasses. The lanthanide spectra contain narrow bands in the visible and near infrared regions, which arises due to transitions between levels of $4f^N$ configuration.

5.1 Energy levels and interaction parameters

The theory of the levels of $4f^N$ configuration has been discussed in detail by Dieke and others. The Perturbed Hamiltonian of the free ion consists of three terms and can be written as –

$$H_e=H_m+H_e+H_c$$

Where: - H_e=Hamiltonian due to electrostatics interaction

H_m=Hamiltonian due to magnetic interaction

H_c=Hamiltonian due to configuration interaction

Considering these interactions within and different configurations, the energy matrices are constructed. The order of the matrices equals the number of levels with a particular

value of J. Details of the methods have been described by Wybourne, Carnall, Hufner, Morrison and Leavitt.

5.1.1 Electrostatic interaction

The Hamiltonian for electrostatic repulsion between the outer electrons is given by-

$$H_e = \sum_{i<j}^{N} \frac{e^2}{r^{ij}} \quad (1)$$

Where the summation is over the coordinates of all electron pairs and N is the number of electrons.

Slater and Racah have used slightly different methods to calculate the electrostatic energy E_e.

5.1.1.1 Slater's method:

The matrix elements are generally written as linear combination of slater radial integrals F^K, giving the electrostatic energy E_e as-

$$E_e = \sum_{k=2,4,6} f_k F^k \quad (2)$$

Where k is even and f_k's are the coefficients of the linear combination of 4f radial functions and represent the angular part of the interaction. The direct integrals F_K are given by where 'R' is the 4f radial wave function and i and j correspond respectively to the i^{th} and j^{th} electrons under consideration. In order to avoid large denominators appearing in the matrix elements calculation. Condon and shortly have defined reduced integral F_K given by -

$$F_K=\frac{F_k}{D_k} \quad (3)$$

Where D_k's are the denominators, whose values have been tabulated by Nielson and Coster. The reduced Slater integrals can be written as

$$F_k=\frac{1}{D_k}\int_0^\infty\int_0^\infty \frac{r^k}{r^{k+1}}R_i^2(r_i)R_j^2(r_j)r_i^2r_j^2dr_idr_j \quad (4)$$

These reduced parameters F_2, F_4 and F_6 are known as Slater Condon parameters.

5.1.1.2 Racah's method:

In this method new operators have been introduced which have simple transformation properties under the group transformation employed to classify the wave functions. The electrostatic energy E_e can be written as-

$$E_e=\sum_{k=1}^{3} e_k E^k \quad (5)$$

Here e_k's are expectation values of the new operator. Racah parameters E^k (k=1, 2, 3) can be expressed as linear combination of F_k (k=2,4,6) given by-

$$E^1=(70\ F_2+231\ F_4+2002\ F_6)/9 \quad (6)$$

$$E^2=(F_2-3F_2+7F_6)/9 \quad (7)$$

$$E^3=(5F_2+6F_4-91F_6)/3 \quad (8)$$

It is of interest to note that both F_k(k=2,4,6) and E^k(k=1,2,3) can be treated as parameters and can be determined from observed energy levels.

5.1.2 Magnetic interaction

Pure electrostatic interactions are not sufficient to describe these energy states of lanthanides because many energy levels contain different admixtures of the basis states. The magnetic interactions must be included in the calculations. The magnetic interaction includes the following interactions.

1. Spin-orbit interaction
2. Spin-spin interaction
3. Spin -other orbit interaction
4. Orbit-orbit interaction

Among all these interactions, this spin- orbit interaction has largest magnitude has been described below while other interactions may be neglected.

The Hamiltonian due to spin orbit interaction is given by

$$H_{SO}=\sum_{i=1}^{n} \xi_i(r_i)\,(s_i, Ii) \qquad (9)$$

Where r_i= radial co-ordinates

S_i=Spin angular momentum

I_i= orbital angular momentum

And $\xi_i(r_i)$ is given by -

$$\xi_i(r_i)=\frac{\hbar^2}{2m^2c^2r_i}\frac{dU(r_i)}{dr_i} \qquad (10)$$

Where $U(r_i)$ is the spherically symmetric potential function under central field approximation.

$$\zeta_{4f}=\int_0^{\infty} R_{4f}^2\,\xi(r_i)dr_i \qquad (11)$$

Where ζ_{4f} is a radial integral which is known as Lande's parameter.

The energy E_{SO} corresponding to the Hamiltonian H_{SO} may be written as –

$$E_{SO}=A_{so}\zeta_{4f}$$

Where A_{so} represent the angular part of spin-orbit interaction.

5.1.3 Configuration interaction

It is found that the calculated energy levels for a particular configuration deviate from the observed ones. The reason of this deviation is the neglecting of different configuration of the same parity. These types of interactions are known as configuration interaction. They have origin in the large off- diagonal matrix elements of the electrostatic interaction. Their effect is to shift all the energy states by nearly same amount. Consequently, the energies of f-f transitions do not undergo any significant change due to configuration interactions.

5.1.4 Computation of interaction parameters

Since, the f- orbitals are shielded ones, the variations of energy states is very small with change in environment. Wong and other workers have used Taylor series expansion. It consists of calculating an initial set F_2, F_4 and F_6 and ζ_{4f} by expanding the energy E_j (F_k, ζ_{4f}) as a Taylor series expansion. In the first order approximation the energy E_j of the j^{th} level is given by [28, 29]

$$E_j(F_k,\zeta_{4f})=E_{oj}(F_k^o\zeta_{4f}^o)+\sum_{k=2,4,6}\frac{\partial E_j}{\partial F_k}\Delta F_k+\frac{\partial E_j}{\partial \xi_{4f}}\Delta\zeta_{4f} \quad \text{... (12)}$$

Where E_{oj} is the zero order energy of j^{th} level and ΔF_k and $\Delta\zeta_{4f}$ are the small changes in the corresponding parameters and these values have been calculated by partial regression method.

The values of zero- order energy E_{oj} and partial derivatives $\frac{\partial E_j}{\partial F_k}$ and $\frac{\partial E_j}{\partial \xi_{4f}}$ for observed levels of Pr^{3+} and Nd^{3+} calculated by Wong has been used.

The value of F_k and ζ_{4f} are then evaluated using equations.

$$F_k=F_k^o+\Delta F_k \quad (13)$$

$$\text{And} \quad \zeta_{4f}=\zeta_{4f}^o+\Delta\zeta_{4f} \quad (14)$$

Where F_k^o and ζ_{4f}^o are zero order values of corresponding parameters. The Racah parameters, E^k, have been calculated from F_k parameters.

Using the computed F_k and ζ_{4f} values, the E_j values (E_c) have been calculated for Pr^{3+} and Nd^{3+} doped glasses. The root means square deviation (σ) between calculated (E_c) and observed energies (E_m) of the levels have been calculated. The rms deviation (σ) is defined as-

$$\sigma=\left[\sum_i \Delta E_i^2 X\frac{1}{N}\right]^2 \quad (15)$$

Where ΔE_i is the difference between observed and calculated values of energies of the ith level and N is the number of experimental levels fitted. Small values of σ indicate the justification for calculating parameters.

5.2 Nephelauxetic ratio and bonding parameter

The bands due to electronic transitions have been found to shift to longer wavelengths (red shift) on complexation. In the case of transition metal ions this shift has been explained due to expansion of metal d – orbitals on complexation, resulting in the decrease of interelectronic repulsion parameters. This phenomenon is known as nephelauxetic effect and quantitatively measured in terms of nephelauxetic ratio (β') defined by-

$$\beta' = \frac{F_k^g}{F_k^f} \qquad (16)$$

Where 'g' and 'f' refer to the glass and free ion in the present case respectively.

If the value of β' is less than one. It indicates covalent bonding, while greater than one indicates ionic bonding.

Henrie and Choppin have defined another bonding parameter, $b^{1/2}$ given by-

$$b^{1/2} = \left[\frac{1-\beta'}{2}\right]^{1/2} \qquad (17)$$

A real value of bonding parameter indicates covalent bonding. This parameter is very useful for comparative study of bonding.

5.3 SPECTRAL INTENSITIES

The spectral intensity of a band is generally expressed in termsof oscillator strength P_m. its experimentally measured value is given by-

$$P_m = 4.6X10^{-9} \text{ X } \frac{1}{cl} \log \frac{I_o}{I} \text{ X } \Delta v_{1/2} \qquad (18)$$

Where 'c' is the molar concentration of the absorbing ion per unit volume 'l' is the optical path length, log I_o/I is absorptivity or optical density and $\Delta v_{1/2}$ is half band width.

In case of solids, the spectral intensity is expressed in terms of line strength S_m which is related to oscillator strength 'P_m' by the relation

$$P_m = \frac{8\pi^2 \pi mc\bar{\upsilon}}{3h(2J+1)} \frac{1}{n} \left[\frac{(n^2+2)^2}{9} \right] S_m \qquad (19)$$

Where v is the average energy of the transition in cm^{-1}, J is the total angular momentum of the initial level. The factor $(n^2+2)^2/9$ represents the local field correction for an ion embedded in a dielectric medium of refractive index n, under the tight bonding approximation. Other symbols have their usual meanings.

The oscillator strength, P_m of this transition may be due to electric dipole, magnetic dipole or electric quadrapole or contribution from more than one of these modes. The values of oscillator strength for electric dipole, magnetic dipole and quadrupole transitions are 10^{-11}, 10^{-9} and 10^{-6} respectively. In case of magnetic dipole transition, the f-f transition are parity allowed and in the R-S coupling scheme they follow the

selection rules: $\Delta l=0$, $\Delta S=0$, $\Delta L=0$ and $\Delta J\leq 1$ ($J'=0$ □$J''=0$). This selection rules are also followed by electric quadrupole mode. Due to very small values of oscillator strength for these modes, the contribution is mainly from electric dipole mode.

5.4 Electric dipole transition & Judd- Ofelt theory:

A true electric dipole transition requires the initial and final states to be of different parity, whereas no parity change is involved in transition within a configuration. Hence, the pure electric dipole transitions are forbidden, whereas the magnetic dipole and electric quadrupole transitions are allowed ones.

These were explained by Judd and independently by Ofelt treating them as due to included electric dipole transitions, pure ones being parity forbidden. The asymmetries produced by vibronic coupling of the central metal ion with its surrounding can induce electric dipole transitions. They can also occur due to the interaction of the central rare earth ion with the surrounding ions mixing into the $4f^N$ configuration states from configurations of opposite parity. Thus, relaxing the parity restrictions. On this basis Judd Ofelt expressed the electric dipole line strength as a sum of products of phenomenological intensity parameters Ω_λ, and matrix elements of tensor operators $U^{(\lambda)}$ connecting states of $4f^N$.

For transition between initial J manifold $|4f^N (\alpha, S, L) J\rangle$ and terminal J' manifold $|4f (\alpha', S', L') J'$, the calculated line strength is given by –

$$S_c = \sum_{\lambda=2,4,6} \Omega_\lambda |\langle f^N (\alpha, S, L)\, J \,||U^{(\lambda)}||\, f^N (\alpha', S', L')\, J' \rangle|^2$$

Where , $4f^N$ (α,S,L) $J >$ are basis sates in the LS coupling scheme and α represents an extra quantum number that might be necessary to describe the states completely ,$U^{(\lambda)}$ are the unit tensor operators of the rank λ which are doubly reduced to yield the matrix elements $\langle||U^{(\lambda)}||\rangle$ in the intermediate coupling scheme and Ω_λ are phenomenological Judd – Ofelt parameters , which specify the electric dipole moment between any two electronic levels and contain implicitly the old symmetric crystal filed terms, radial integrals and perturbation denominators.

The Judd- Ofelt theory has been proved to be quite successful for the intensity analysis of the spectra of trivalent rare earth ions. It was originally applied to the solution spectra of Rare Earth ions by Carnall and coworker. Tandon and coworkers and later on it was extended to the rare earth ions in powder state. Weber, Reisfeld and Tandon groups have tried to extend it in the case of glasses.

CHAPTER 6
LASER PARAMETERS AND PHYSICAL PROPERTIES OF RE^{3+} DOPPED GLASSES

The detailed study of laser parameters indicates which of the following fluorescence transitions probable laser transitions are. It is essential that the laser material should show strong fluorescence. We know that on excitation from ground state the atom reaches an excited state, from which it may be immediately come down to ground state or go to another excited metastable state of lower energy by non-radiative process. From this state it comes down to another state by radiative process. This radiative transition is known as fluorescence.

What are the fluorescence spectra?

The fluorescence spectra of the rare earth ions appear due to radiative decay mechanism. The decay of energy state occurs by decoupling of the dipole moments in the rare earth ion connecting the excited metastable state and other lower states. It is well known that the width of the fluorescence bands depends on the composition of host glasses.

6.1 Laser Parameters

The radiative properties of rare earth ions have been expressed in terms of certain parameters often called as Laser parameters by Krupke and Jacobs and Weber. They are related to Judd-Ofelt intensities parameters and fluorescence data of these ions. They are very useful in predicting laser action in rare earth ions doped glass- specimens. They are widely used by Weber, Reisfeld, Laxman and Tandon groups. They are discussed below: -

6.1.1 Spontaneous Emission Probability (A)

The spontaneous emission probability from an initial manifold $|f^N (\alpha', S', L') J'>$ to a terminal manifold $|f^N (\bar{\alpha},\bar{S},\bar{L})\bar{J}>$ is given by –

$$A=\frac{64\pi^4 e^2}{3h(2J'+1)\lambda_p^3} n\left[\frac{(n^2+2)^2}{9}\right] X \sum_{\lambda=2,4,6} \Omega_\lambda |<f^N(\alpha',S',L')J'||U^{(\lambda)}||f^N(\bar{\alpha},\bar{S},\bar{L})\bar{J}>|^2$$

Where the symbols have usual meanings. The A values for different emission transitions, are calculated by substituting the emission wavelength λ_p, reduced matrix elements for the relevant transition and the values of Ω_λ parameters.

6.1.2 Fluorescence Branching Ratio (β)

The fluorescence branching ratio (β)for the transitions originating from a specific initial manifold $|f^N(\alpha',S',L')J'>$ is defined as –

$$\beta=\frac{A}{\sum_{\alpha,S,LJ} A}$$

where A is the spontaneous emission probability for the transition from an initial manifold $|f^N(\alpha',S',L')J'>$ to a terminal manifold $|f^N(\bar{\alpha},\bar{S},\bar{L})\bar{J}>$. The β values depend upon Ω_4, Ω_6 parameters which in turn depend upon the glass composition.

6.1.3 Radiative Lifetime (τ)

The radiative life time τ for a transition is a reciprocal of spontaneous emission probability A. For radiative decay from the initial J' manifold $|f^N(\alpha',S',L')J'>$ it is given by -

$$\tau = A^{-1}$$

The τ values have been calculated for all the relevant transitions of rare earth ions in different hosts.

6.1.4 Stimulated Emission Cross – section (σ_p)

The stimulated emission cross- section (σ_p) for transition from an initial J manifold $|f^N(\alpha',S',L')J'>$ to terminal J manifold $f^N(\bar{\alpha}',\bar{S}',\bar{L}')\bar{J}'>$ is expressed as –

$$\sigma_p = \frac{\lambda_p^4}{8\pi c n^2 \Delta\lambda_{eff}} A$$

where λ_p is the peak fluorescence wave length of the emission band and $\Delta\lambda_{eff}$ is the effective fluorescence line width, which is a measure of a combination of the extend of the stark splitting of the initial and terminal J manifold and the inhomogeneous broadening resulting from the site – to – site variation of the local field

$$\Delta\lambda_{eff} = \frac{\int I(\lambda) d\lambda}{I_{max}}$$

Where I(λ) is fluorescence intensity at wavelength λ.

The rate of energy excitation from a laser material is dependent on the stimulated emission cross- section σ_p. This parameter is most important among laser parameters and is generally used to predict laser action in glass specimens. The importance of σ_p lies in the fact that it gives a relationship between lasing action to spectral/optical parameters viz. fluorescence peak wavelength, effective linewidth, spontaneous emission probability, and the refractive index.

6.2 Theoretical properties

6.2.1 Nephelauxetic ratio(β) and bonding parameter ($B^{1/2}$)

The nature of the R-O bond is known by the Nephelauxetic Ratio (β)and Bonding parameter (δ), which can be computed by using following formulae. The Nephelauxetic Ratio is given by –

$$\beta=\frac{\upsilon_g}{\upsilon_a}$$

where, ν_g and ν_a refer to the energies of the corresponding transition in the glass and free ion, respectively. The values of bonding parameter δ is given by-

$$\delta= \frac{1-\bar{\beta}}{\beta}$$

where $\overline{\beta}$ is the average value of β.

6.2.2 The Oscillator Strengths

The intensity of spectral lines can be expressed in terms of oscillator strengths using relation

$$f_{exp}=4.32X10^{-9}\int \varepsilon(\nu)d\nu$$

where, ε(ν) is molar absorption coefficient at a given energy ν (cm^{-1}), to be evaluated from Beer- Lambert law.

Under Gaussian Approximation, using Beer- Lambert law, the observed oscillator strengths of the absorption bands can be experimentally calculated using the modified relation:

$$f_{exp}= 4.6X10^{-9} X \frac{1}{cl}\log\frac{I_o}{I} X \Delta\nu_{1/2}$$

where c represents the concentration of rare earth ion in the glass and 'l' is the optical path length. $\log \frac{I_o}{I}$ is called optical density, $\Delta\nu_{1/2}$ is the half band width. The intensities of all the bands can be measured by the area method.

6.2.3 Judd- Ofelt Parameters

According to Judd Ofelt theory, independently derived expression for the oscillator strength of the induced forced electric dipole transitions between an initial J manifold $|4f^N(S,L)J>$ level and the terminal J' manifold $|4f^N (S',L')J'>$ is given by:-

$$f_{JJ'}= \frac{8\pi^2 mc\nu}{3h(2J+1)}\left[\frac{(n^2+2)^2}{9n}\right]X\ S(J,J')$$

where, the line strength S(J,J') is given by the equation

$$S(J,J') = e^2 \sum_{\lambda=2,4,6} \Omega_\lambda \langle 4f^N(S,L) J \| U^{(\lambda)} \| 4f^N(S',L') J' \rangle^2$$

In the above equation m is the mass of an electron, c is the velocity of light, ν is the wave number of the transition, h is the Planck's constant, n is the refractive index, J and J' are the total angular momenta of the initial and final level respectively, Ω_λ (λ=2,4 and 6) are known as Judd- Ofelt intensity parameters which contain the effect of the old-symmetry crystal field terms, radial integrals and energy denominators. $\|U^{(\lambda)}\|^2$ are the matrix elements of the doubly reduced unit tensor operator calculated in intermediate coupling approximation. Ωλ parameter can be obtained from least square fitting method.

6.2.4 Radioactive Properties

The Ω_λ parameters can be obtained using the absorption spectral results to predict radioactive properties such as spontaneous emission probability (A) and radioactive lifetime (τ_R), and laser parameters like fluorescence branching ratio (β_R) and stimulated emission cross section (σ_p).

The spontaneous emission probability from initial manifold $|4f^N (S',L')J'\rangle$ to a final manifold $|4f^N (\bar{S}, \bar{L})\bar{J}\rangle|$ is given by:

$$A\left[\left(S', L'\right)J'; (\bar{S}, \bar{L})\,\bar{J}\right] = \frac{64\,\pi^2\nu^3}{3h(2J'+1)}\left[\frac{n(n^2+2)^2}{9}\right] XS(J', \bar{J})$$

Where, $S(J', \bar{J}) = e^2 [\Omega_2\|U^{(2)}\|^2 + \Omega_4\|U^{(4)}\|^2 + \Omega_6\|U^{(6)}\|^2]$

For Pr^{3+} ion, J'=0 and 1 matrix elements of the doubly reduced unit tensor operator.

The fluorescence branching ratio for the transitions originating from a specific initial manifold $|4f^N(S',L')J'>$ to a final manifold $|4f^N(\bar{S}, \bar{L})\bar{J}>$ is given by –

$$\beta[(S',L')J';(\bar{S}, \bar{L})\bar{J} = \frac{A[(S',L')J';(\bar{S}, \bar{L})J]}{\sum_{\bar{S},\bar{L},\bar{J}} A[(S',L')J';(\bar{S},\bar{L})\bar{J}]}$$

where, the sum is over all terminal manifolds. In the case of Pr^{3+} ion, the terminal manifold are $^3P_2$, $^1I_6$, $^3P_{1,0}$, $^1D_2$,$^1G_4$, $^3F_{4,3,2}$ and $^3H_{6,5,4}$.

The radioactive life time is given by-

$$\tau_{rad} = \sum_{\bar{S},\bar{L},\bar{J}} A[(S', L')J'; (\bar{S}, \bar{L})\bar{J}]^{-1} = A^{-1}_{total}$$

where, the sum is over all possible terminal manifolds.

The stimulated emission cross – section for a transition from an initial manifold $|4f^N(S',L')J'>$ to a final manifold $|4f^N(\bar{S},\bar{L})\bar{J}>|$ is expressed as –

$$\sigma_p(\lambda_p) = \left[\frac{\lambda_p^4}{8\pi n^2 \Delta\lambda_{eff}}\right] X\ A[\ (S',L')J';(\bar{S},\bar{L})\bar{J}]$$

where, λ_p, is the peak fluorescence wavelength of the emission band and $\Delta\lambda_{eff}$ is the effective fluorescence line width.

6.2.5 Physical PropertiesRare Earth Ions Concentration:

The rare earth ions concentration can be measured by-

$N(ions/cm^3)=\frac{(Avogadro's number)(glass\ density)}{(Average\ molecular\ weight)}$X mol% of rare earth

6.2.6 Dielectric Constant:

The dielectric constant (ε) can calculate from the refractive index of the glass using

$$\varepsilon = n_d^2$$

6.2.7 Optical Dielectric Constant:

The optical dielectric constant can calculate from the measured refractive index using the formula.

$$p\frac{\partial t}{\partial p} = (\varepsilon\text{-}1) = (n_d^2\text{-}1)$$

where, ε is the dielectric constant.

From the average molecular weight of the glass, the density and the total number of ions the mean atomic number (in g/cm^3/atom) can be obtained.

6.2.8 Reflection Loss:

The reflection loss from the glass surface can compute from the refractive index by using the Fresnel formula as shown below-

$$R=\left[\frac{n_{d-1}}{n_{d+1}}\right]^2$$

6.2.9 Molar Refractivity:

The molar refractivity R_m for each glass can be evaluated using

$$R_m = \left[\frac{n_d^2 - 1}{n_{d+1}^2}\right]\frac{\overline{M}}{D}$$

Where, M is the average molecular weight and D is the density in g cm^{-3}.

6.2.10 Polar Radius and Inter Ionic Separation:

The polaron radius and inter-ionic separation can calculate using the formula

$$r_p = \frac{1}{2\left(\frac{\pi}{6N}\right)^{\frac{1}{3}}}$$

And,

$$r_i = \left(\frac{1}{N}\right)^{1/3}$$

6.2.11 Electronic Polarizability:

The electronic polarizability α_e was calculated using the formula

$$\alpha_e = \frac{3\left(n_d^2 - 1\right)}{4\pi N\left(n_d^2 + 2\right)}$$

Where, N is the rare earth ions concentration.

6.2.12 Molar Volume:

The molar volume (V_m) of the glass samples can be calculated from the molecular weight (M) and density (ρ) using the following relation

$$V_m = \frac{M}{\rho}$$

6.2.13 Oxygen Packing Density:

The oxygen packing density (O), ionic concentration (N) of Zn^{2+} ions and inter ionic distance (R) can be calculated using the following relations

$$O = \frac{\rho}{m} X\ n$$

$$N = \frac{6.023\ X\ a\ X\ b}{V_m}$$

$$R = \left(\frac{1}{N}\right)^{1/3}$$

Where n is the number of oxygen atoms per formula unit, as is the mol% of caution and b is the valiancy of the cautions.

CHAPTER 7
APPLICATION OF GLASSES

Ceramic glasses play important role in the construction industry as bricks, tiles and pipes. They are also used in road construction due to their resistance to wear and tear.

Ceramic materials are used in **engine manufacture** to minimize the chances of thermal damage. They are used in making engine combustion chamber components, like cylinder liners, piston top injection, etc. The engine can reduce heat loss and reduce fuel consumption after this treatment.

Ceramic products are widely used in **consumer electronics**: As insulators in various applications, including spark plugs, hermetic packaging, ceramic arc tubes, and protective elements like beads and tubing for bare wires and power lines.

Ceramics glasses also use in the **aerospace industry** include brakes, bearings, seals, and other wear resistant components; armor for helicopters; electronic thermal management structures; lightweight optical components (e.g., silicon carbide mirrors); radiators (i.e., cooling systems) for space vehicles.

Ceramics glasses use in **medical** instruments and tools, including tissue engineering scaffolds, medical pumps, blood

shear valves for hematology testing, drug delivery devices, piezoelectric components for medical tools and instruments; and ceramic-to-metal assemblies for imaging.

Ceramic glasses are used in different optical instrument like as lenses for analytical and medical equipment, photographic lances, windows for optical system and instruments, glass substrates, lead radiation glasses precision lenses, pressure sensors, laser systems and beam splitters. Ceramic glasses does not directly affected by magnetic field this property make a special use in future research equipment.

Chapter 8

References

1. M. Wachter, A. Speghini , K. Gotterer , H.P. Fritzer, D. Ajo, M. Bettinelli, J. Am. Ceram. Soc. 81 (1998) 2045.
2. C. B. Layne, W.H. Lowdermilk, M.J. Weber, Phys. Rev. B 16 (1997) 10.
3. H. Ebendorff- Heidepriem, D. Ehrt, M. Bettineli, A. Speghini, SPIE proceedings, Belhngham, Washington, USA, 3622 (1999) 19.
4. Am. Soc. Testing Mater, ASTM C 162-56, ASTM stand. Part 13, 1965.
5. P. G. Debenedetti, F. H. Stillinger, Nature 410 (2001) 259.
6. J.O. Keefe, W. Weiss- Kirchner, Glasstechn. Ber.43 (1970) 199.
7. J. Zarzycki, “Glasses and the Vitreous State”, Cambridge University press, Cambridge, 1991.
8. R. W. Douglas, J. Sci. Instrum., 22 (1945) 81.
9. J. D. Main – Smith, Nature (London) 120 (1927) 583.
10. S. P. Tandon, A. Gokhroo, SSL Surana and M.P. Bhutra and K. Tondon. Ind. J. pure appl. Phys. 30 (1992) 67.
11. L. Boehm, R. Reisfeld and N. Spector. J. Solid State Chem. 28 (1979) 75.
12. R. Reisfeld, Proc. Topical Meeting of Tunable Solid State Lasers, Cape Code, Massachusetts (USA) (1989).

13. Y. K. Sharma, Spectral and Electrical Properties of Lanthanide ions in Different Environment, Ph.D. Thesis. The University of Jodhpur, Jodhpur India (1990).
14. N. B. Bishnoi, Spectral and Electrical Properties of Ions in Complexes and Glasses, Ph.D. Thesis, The University of Jodhpur, India (1990).
15. Y. K. Sharma, N. B. Bishnoi, S. S. L. Surana and S. P. Tandon, J. Pure Appl. Phys. India, 4, 200 (1992).
16. R. C. Sagar, Spectral Behaviour of Lanthanide ions in Glassy Matrix, Ph. D. Thesis, Jai Narain Vyas University, Jodhpur, India (1995).
17. M.Hanumanthu, K. Annapurna and S. Buddhudu. Solid StatComm. 80, 315 (1991).
18. V. D. Rodriguez, I. R. Martia, R. Alcala and R. cases. J. Lumin 54, 231 (1992).
19. R. Reisfeld, Proc. Topical Meeting Of Tunable Solid State Lasers, Cape Code, Massachusetts (USA) (1989).
20. Y. K. Sharma, Spectral and Electrical Properties of Lanthanide ions in Different Environment, Ph. D. Thesis. The University of Jodhpur, Jodhpur India (1990).
21. N. B. Bishnoi, Spectral and Electrical Properties of Ions in Complexes and Glasses, Ph.D. Thesis, The University of Jodhpur, India (1990).
22. Y.K. Sharma, N. B. Bishnoi, S. S. L. Surana and S. P. Tandon, J. Pure Appl. Phys. India, 4, 200, (1992).
23. M. C. Sharma, Study of Laser Parameters of Lanthanide Doped Glasses, Ph. D. Thesis, Jai Narain Vyas University, Jodhpur, India (1998).

24. Y. K. Sharma, D. C. Dube and S. P. Tandon, Materials Science Forum, Switzerland 223, 105 (1996).
25. Y. K. Sharma, M. C. Sharma, S. S. L. Surana and S.P. Tandon, Proceedings of International Conference on Physics od Disordered Materials, Jaipur, Eds., M.P. Sexena, N. S. Saxena and D. Bhandari, NISCOM, New Delhi, India, 32 (1997).
26. S. P. Tandon, Y. K. Sharma, N. B. Bishnoi and K. Tandon, Def. Sci. J. India, 47, 225 (1997).
27. Y. K. Sharma, S. P. Tandon, S. S. L. Surana, M. C. Sharma and C. L. Gehlot, Can. J. Anal. Sci. Spectrose., 45, 66 (2000).
28. Y. K. Sharma, S. P. Tandon and S. S. L. Surana, J. Mat. Sci. Engg, B77, 167, (2000).
29. S. S. L. Surana, Y. K. Sharma and S. P. Tandon, J. Mat. Sci. Engg. India, B83, 204 (2001).
30. S. S. L. Surana, C. L. Gehlot, S. P. Tandon and Y. K. Sharma, Can. J. Anal. Sci. &Spectrosc., 48, 285 (2003).
31. Y. K. Sharma, S. S. L. Surana, C. L. Gehlot and S. P. Tandon, Indian J. Engg. & Mat. Sci., 10, 215 (2003).
32. S.P. Tandon, Y. K. Sharma, N. B. Bishnoi and K. Tandon, Def. Sci. J., India, 47, 225 (1997).
33. Y. K. Sharma, S. P. Tandon and S. S. L. Surana, J. Mat. Sci. Engg, B77, 167 (2000).
34. M. J. Weber and R. M. Almeida, J. Non- cryst. Solids 43, 99 (1981).

35. M. C. Sharma, Study of Laser Parameters of Lanthanide Doped Glasses, Ph.D. Thesis, Jai Narain Vyas University, Jodhpur, India (1996).
36. J. Fu and H. Yastsuda , Phys. Chem. Glasses. 36, 211 (1995) A. Pan and A. Ghosh, A. Pan and A. Ghosh, J. Non- Cryst. Solid. 271,157 (2000).
37. C. Stehle, C. Vira, D. Hogan, S. Feller, and M. Affatigato, Phys. Chem. Glasses. 39 ,83 (1998).
38. S. Sindhu, S. Sanghi, A. Agarwal, V. P. Seth, and N. Kishore, Matter. Chem. Phys. 90, 83 (2005).
39. G. Sharma, K. Singh, Manupriya, S. Mohan, H. Singh and S. Bindra, Radiat. Phys. Chem. 75, 959 (2003).
40. E. F. Lambson, G. A. Saunders, B. Bridge, R. A. El-Mallawany, The elastic behaviour of TeO_2 glass under uniaxial and hydrostatic pressure. J. Non- Cryst. Solids 69, 117-133 (1984).
41. H. A. A. Sidek, R. EL – Mallawany, S. Rosmawati , A. K. Yahya, Characteristics temperatures and microhardness of $(ZnO)_X$ – $(AlF_3)_y$- $(TeO_2)_Z$ tellurite glass systems. Chalcogenide Lett. 13, 169-176 (2016).
42. G. Ghosh, Sellmeier coefficients and chromatic dispersions for some Tellurite glasses. J. Am. Ceramic. Soc. 78,2828-2830 (1995).
43. R. El- Mallawany, A. Patra, C. S. Friend, R. Kapoor, P. N. Prasad, Study of luminescence properties of Er^{3+} - ions in new tellurite glasses, Opt. Mater. 26,267-270 (2004).

44. F. Yang, C. Liu, D. Wei. Y. Chen, J. Lu., S. -e. Yang, Er^{3+}-Yb^{3+} co doped TeO_2- PbF_2 oxyhalide tellurite glasses for silicon solar cells. Opt. Mater. 36, 1040-1043 (2014).
45. J. Qin, W. Zhang, S. Bai, Z. Liu, Effect of Pb- Te- O glasses on Ag thick – film contact in crystalline silicon solar cells. Sol. Energy Mater. Sol. Cells 144, 256- 263 (2016).
46. L. Wu., Y. Zhou, Z. Zhou, P. Cheng, B. Huang, F. Yang, J. Li, Effect of silver nanoparticles on the 1.53 μm fluorescence in Er^{3+} / Yb^{3+} co doped tellurite glasses. Opt. Mater. 57, 185-192 (2016).
47. M. Boscaa, L. Pop, L. Bolundut , N. Tothazan, G. Borodi, I. Vida- Simiti, R. Stefan, A. Popa, E. Culea, P. Pascuta, Effects of Gd^{3+} : Ag co – doping on structural and magnetic properties of lead tellurite glass Ceramics. Ceram. Int. 42, 1169- 1117 (2016).
48. D. Li., W. Xu, P. Kuan, W. Li., Z. Lin, X. Wang, L. Zhang, C. Yu, K. Li, H. Lili, Spectroscopic and laser properties of Ho^{3+} doped lanthanum – tungsten- tellurite glass and fiber. Ceram. Int. 42, 10493- 10497 (2016).
49. L. M. Moreira, V. Anjos, M. J. V. Bell, C. A. R. Ramos, L. R. P. Kassab, D. J. L. Doualan, P. Camy, R. Moncorge, Nd^{3+} - doped TeO_2 – PbF_2 – AlF_3 Opt. Mater. 58, 84-88 (2016).
50. J. Han, S. Li., T. Zhang, Design on a novel hybrid- core photonic crystal fiber with large birefringence and high nonlinearity. Optical and Quantum Electronics. 48, 371-376 (2016).

51. A. Mori, Tellurite – based fibers and their applications to optical communication networks. J. Ceram. Soc. Jpn. 116, 1040- 1051 (2008).
52. M. I. Sayyed, H. Elhouichet, Variation of energy absorption and exposure build up factors with incident photon energy and penetration depth for boro – tellurite (B_2O_3- TeO_2) glasses. Radiat. Phys. Chem. 130, 335- 342 (2017).
53. N. Berwal, S. Dhankhar, S. Preeti, R. S. Kundu, R. Punia, N. Kishore, Physical, structural and optical characterization of silicate modified bismuth- borate – tellurite glasses. J. Mol. Struct. 1127, 636-644 (2017).
54. M. M. El- Zaidia, A. A. Ammar, R. A. El- Mallwany, Infra – red spectra, electron spin resonance spectra, and density of (TeO_2)100 – x - (WO_3)x and (TeO_2)100-x – ($ZnCl_2$)x glasses. Phys. Status Solidi A 91 (2) , 637- 642 (1985).
55. A. Abdel- Kader, , R. El-Mallawany, M. M. Elkholy, Network structure of tellurite phosphate glasses: Optical absorption and Infrared spectra. J. Appl. Phys. 73(1),71-74 (1993).
56. I. Z. Hager, R. El- Mallawany, A. Bulou, Luminescence spectra and optical properties of TeO_2 - WO_3 – Li_2Oglasses doped with Nd, Sm and Er rare earth ions. Physica B : Condensed Matter 406 (4), 972-980 (2011) 406 (4), 1844 (2011).

57. I. Z. Hager, R. El – Mallawany, Preparation and structural studies in the (70 - x) TeO_2 – 20 WO_3 – 10 Li_2O – x Ln_2O_3 glasses. J. Mater.Sci. 45(4), 897 (2010).
58. N. S. Hussain, G. Hungerford, R. El- Mallawany , M. J. M. Gomes, M. A. Lopes, N. Ali, J. D. Santos, S. Buddhundu, Absorption and emission analysis of RE^{3+} (Sm^{3+} and Dy^{3+}) : Lithium Boro Tellurite glasses. J. Nanosci. Nanotechnol. 9 (6), 3672- 3677 (2009).
59. R. El- Mallawany, M. Sidkey, A. Khafagy, H. Affiti, Ultrasonic attenuation of tellurite glasses. Mater. Chem. Phys. 37 (2), 197- 200 (1994).
60. M.M. Elkholy,R. A. El- Mallawany, Ac conductivity of tellurite glasses. Mater. Chem. Phys. 40(3), 163-167 (1995).
61. A. El- Adawy, R. El – Mallawany, Elastic modulus of tellurite glasses. J. Mater. Sci. Lett.15(23), 2065-2067 (1996).
62. H. M. M. Moawad, H. Jain, R. El- Mallawany , T. Ramadan, M. El- Sharbiny, Electrical conductivity of silver vanadium tellurite glasses. J. Am. Ceram. Soc. 85 (11), 2655- 2659 (2002).
63. R. El – Mallawany, Specific heat capacity of semiconducting glasses: Binary vanadium tellurite. Phys. Status Solidi A 177(2), 439- 444 (2000).
64. R. El – Mallawany, A. Abd El – Moneim, Comparison between the elastic moduli of tellurite and phosphate glasses. Phys. Status Solidi A 166 (2), 829-834 (1998).

65. R. El- Mallawany, A. H. El – Sayed, M. M. HA El-Gawad, ESR and electrical conductivity studies of (TeO_2) 0.95 (CeO_2) 0.05 semiconducting glasses. Mater. Chem. Phys. 41(2), 87-91 (1996).
66. H. M. M. Moawad, H. Jain, R. El- Mallawany, DC conductivity of silver vanadium tellurite glasses. J. Phys. Solids 70(1), 224-233 (2009).
67. R. El- Mallawany, Theoretical analysis of the electrical properties of tellurite glasses. Mater. Chem. Phys. 37(4), 376- 381 (1994).
68. R. El – Mallawany, Phase separation ultrasonic detection of micrphase separation in Tellurite glasses. Phys. Stat. Soli. (a) 133, 245 (1992).
69. A. Mirgorodsky, M. Colas, M. Smirnov, T. Merle-Mejean, R. El- Mallawany, Philippe Thomas, structural peculiarities and Raman spectra of TeO_2/ WO_3 – based glasses: A fresh look at the problem. J. Solid state Chem. 190, 45-51 (2012).
70. R. El- Mallawany, M. Sidkey, A. Khafagy, H. Affifi, Elastic constants of semiconducting tellurite glasses. Mater. Chem. Phys. 37 (3), 295- 298 (1994).
71. Sidky, R. El – Mallawany, R. Nakhala, A. El-Moneim,Ultrasonic attenuation at low temperature of TeO_2 – V_2O_5 glasses. Phys. Stat. Soli. (a) 159, 397 (1997).
72. R. El- Mallawany, Theoretical analysis of ultrasonic wave attenuation and elastic moduli of Tellurite glasses. Mater. Chem. Phys. 39,161 (1994).

73. R. El- Mallawany, H. M. Diab, Improving dosimetric properties of tellurite glasses. Phys. B Condens. Matter 407 (17), 3580-3585 (2012).
74. M. A. Merzliakov, V. V. Kouhar, G. E. Malashkevich, E. V. Pestryakov, Spectroscopy of Yb- doped tungsten – tellurite glass and assessment of its lasing properties. Opt. Mater. 75, 142- 149 (2018).
75. R. El- Mallawany, M.S. Gaafar, M. A. M. Abdeen, S.Y. Marzouk, Simulation of acoustic properties of some tellurite glasses. Ceram. Int. 40, 7389-7394 (2014).
76. M. A. Sidky, R. A. El- Mallawany, A. A. Abously, Y. B. Saddeek, Relaxation of longitudinal ultrasonic waves in some tellurite glasses. Mater. Chem. Phys. 74(2), 222-229 (2002).
77. R. El- Mallawany, Devitrification and Vitrification of Tellurite glasses. J. Mater. Sci. Elect. 6 (1) (1995).
78. R. A. El- Mallawany, L. M. Sharaf El- Deen, M. M. Elkholy, Dielectric properties and polarizability of molybdenum, tellurite glasses. J. Mater. Sci. 31 (23), 6339- 6343 (1996).
79. R. El – Mallawany, Debye temperature of ternary tellurite glasses at room temperature. Phys. Status Solidi A 130 (1), 103- 108 (1992).
80. V. Uma, M. Vijaykumar, K. Marimuthu, G. Muralidharan, Luminescence and energy transfer studies on Sm^{3+}/ Tb^{3+}codoped telluroborate glasses for WLED applications. J. Mol. Struct. 1151, 266-276 (2018).

81. D. S. da Silva, N. U. Wetter, W. de Rossi, L. R. P. Kassab, R. E. Samad, Production and characterization of femtosecond laser- written double line waveguides in heavy metal oxide glasses. Opt. Mater. 75, 267-273 (2018).
82. Y. Sun, Q. Yang, H. Wang, Y. Shao, Sensitization of Ho^{3+}on the 2.7 μm emission of Er^{3+}in $(Y\ 0.9La0.1)_2\ O_3$ transparent ceramics. J. Lumin. 194, 50- 55 (2018).
83. R. El – Mallawany, H. A. Afifi, M. El- Gazery, A. A. Ali, Effect of Bi_2O_3 addition on the ultrasonic properties of pentaternary borate glasses. Measurement 116, 314-317 (2018).
84. V. HimamaheswaraRao, P. Syam Prasad, M. Mohan Babu, P. Venkateswara Rao, T. Satyanarayana, L.F. Santos, N. Veeraiah, Spectroscopic studies of Dy^{3+}ion doped tellurite glasses for solid state lasers and white LEDs. Spectrochim. Act A Mol. Biomol. Spectrosc. 188, 516 – 524 (2018).
85. M. E. Alvarez – Ramos, J. Alvarado – Rivera, M. E. Zayas, U. Caldino, J. Hern_ andez – Paredes, Yellow to orange- reddish glass phosphors: Sm^{3+}, Tb^{3+} and Sm^{3+}/Tb^{3+} in zinc tellurite- germanate glasses. Opt. Mater. 75. 88-93 (2018).
86. S. H. Alazoumia, S. A. Aziza, R. El – Mallawany, U. Sa'adAliyud, H. M. Kamari, M. H. M. M. Zaida, K.A. Matoria, A. Ushah, Optical properties of zinc tellurite glasses. Resul. Phys. 9, 1371- 1376 (2018).

87. A.Tubtimate, S. Phadungdhitidhada, D. Wongratanaphisan, A. Gardchareon, S. Choopun, Tailoring Cu2_ xTe quantum – dot – decorated ZnO nanoparticles for potential solar cell applications. Appl. Phys. 14,772- 777 (2014).
88. O. A. Zamyatin, M. F. Churbanov, J. A. Medvedeva, S. A. Gavrin, E. V. Zamyatina, A. D. Plekhovuch, Glass-forming region and optical properties of the TeO2- ZnO-NiO system. J. Non – Cryst. Solids 479, 29-41 (2018).
89. R. El – Mallawany, Evaluation of optical parameters of some tellurite glasses. Optik- Int. J. Light Electron Opt. 125 (20), 6344- 6346 (2014).
90. S. H. Elazoumi, H. A. A. Sidek, Y. S. Rammah, R. El-Mallawany, M. K. Halimah, K. A. Matori, M. H. M. Zaid, Effect of PbO on optical properties of tellurite glass. Res. Phys. 8, 16-25 (2018).
91. R. El- Mallawany, Y. S. Rammah, A. El Adawy, Z. Wassel, Optical and thermal properties of some Tellurite glasses. Am. J. Opt. Photon. 5(2), 11-18 (2017).
92. A. Abdel Kader, A. Higazy, R. El- Mallawany, M. Elkholy, The effect of gamma irradiation on the electrical conductivity of TeO_2- P_2O_5 and Bi_2O_2 - TeO_2- P_2O_5 glasses. Radiat. Eff. Defects Solids 124, 401 (1992).
93. R. A. H. El- Mallawany, Tellurite Glasses Handbook: Physical Properties and Data, 1st edn. (CRC Press, Boca Raton, 2002.), 2nd Ed.(2011).

94. M. R. Dousti, R. J. Amjad, M. R. Sahar, Z. M. Zabidi, A. N. Alias, A. S. S. De Camargo, J. Non- Cryst. Solids 429, 70-78 (2015).
95. I. Jlassi, H. Elhouichet, M. Ferid, C. Barthou, J. Lumin. 130, 2394-2401 (2010).
96. R. El- Mallawany, J. Appl. Phys. 72, 1774 (1992).
97. H. Zhan, A. Zhang, J. He, Z. Zhou, J. Si, A. Lin. Appl. Opt. 52, 9-11 (2013).
98. K. Kumar, S. B. Rai, D. K. Rai, Solid State Communication 139 (2006) 363.
99. H. T. Amorim, M. V. D. Vermelho, A. S. Gouveia- Neto, F. C. Cassanjes, S. J. L. Ribeiro, Y. Messaddeq, Solid State Chemistry 171 (2003) 278.
100. G. A. Kumar, N. V. Unnikrishnan, Physics and chemistry of glasses 40 ,217 (1989).
101. B. Viana, M. Palazzi, O. Lefol, J. Non- Cryst. Solids. 96, 215 (1997).
102. Y. Zhou, Y. Yang, F. Huang, J. Ren, S. Yuan, G. Chen, J. Non- Cryst. Solids 386, 90 (2014).
103. A. Miguel, M. A. Arriandiaga, R. Morea, J. Fernandez, J. Gonzalo, R. Balda, Journal of Luminescence, 158 ,142 (2015).
104. A. Awang, S. K. Ghoshal, M. R. Sahar, R. Arifin, Optical Materials, 42, 495 (2015).
105. I. Z. Hager, R. El – Mallawany, A. Bulou, Physica B: Condensed Matter 406, 972 (2011).

106. O. Ravi, C. Madhukar Reddy, B. Sudhakar Reddy, B. Deva Prasad Raju, Optics Communications ,312, 263 (2014).
107. E. A. Mohamed, F. Ahmad, K. A. Aly, Journal of Alloys and Compounds 538, 230 (2012).
108. H. Gebavi, D. Milanese, R. Balda, S. Taccheo, J. Fernandez, J. Lousteau, M. Ferraris, Journal of Luminescence 132, 270 (2012).
109. E. F. Chillcce, I. O. Mazali, O. L. Alves, L. C. Barbosa, Optical Materials, 33, 389 (2011).
110. R. Singh, J. S. Chakravarthi, Phys. Rev. B 55, 5550, (1997).
111. V. R. Kumar, N. Veeraiah, J. Materials Science Letters, 16, 1816 (1997).
112. EI. S. Yousef, A. El- Adawy, N. El Koshkhany, E. R. Shaaban, J. Phys. Chem. Solids, 67, 1649 (2006).
113. K. Kumar, S. B. Rai, D. K. Rai, Spectrochim. Acta. Part A, 66, 1052 (2007).
114. J. Ozdanova, H. Ticha, L. Tichy, J. Non – Cryst. Solids ,353, 2799 (2007).
115. G. Qin, R. Jose, Y. Ohishi. J. Appl. Phys. ,101, 093109, (2007).
116. B. C. Jamalaiah, M. V. Vijaya Kumar, K. Rama Gopal, Investigation on luminescence and Energy transfer in Tb^{3+}- doped lead telluroborate glasses, Physica B, 406 , 2871 – 2875 (2011).
117. B. C. Jamalaiah, M. V. Vijaya Kumar, K. Rama Gopal, Fluorescence properties and energy transfer mechanism

of Sm^{3+} ion in lead telluroborate glasses, Optical Material, 33, 1643 – 1647, (2011).

118. M. V. Vijaya Kumar, B. C. Jamalaiah, K. Rama Gopal, R. R. Reddy, Novel Eu^{3+} - doped lead telluroborate glasses for red laser source applications, Journal ofSolidState Chemistry, 184, 2145 – 2149, (2011).
119. M. V. Vijaya Kumar, B. C. Jamalaiah, K. Rama Gopal, R. R. Reddy, Optical absorption and fluorescence studies of Dy^{3+} - doped lead telluroborate glasses, Journal of Luminescence, 132, 86 – 90,(2012).
120. K. Annapoorani, K. Maheshvaran, S. ArunKumar, N. Suriya Murthy, TeroSoukka, K. Marimuthu, Structural and spectroscopic behavior of Er^{3+}: Yb^{3+} co – doped lithium telluroborate glasses, Physica B, 457, 66 – 77, (2015).
121. K. Annapoorani, N. Suriya Murthy, T. R. Ravindran, K. Marimuthu, Influence of Er^{3+} - ion concentration on spectroscopic properties and luminescence behavior in Er^{3+} doped Strontium telluroborate glasses, Journal of Luminescence, 171, 19 – 26, (2016).
122. K. Annapoorani, K. Marimuthu, Spectroscopic properties of Eu^{3+} ions doped Barium telluroborate glasses for red laser applications, Journal of Non – Crystalline solids, 463, 148 – 157 (2017).
123. M. S. Sajna, Subash Gopi, V. P. Prakashan, M. S. Sanu, Cyriac Joseph, P. R. Biju, Spectroscopic investigations and phonon side band analysis of Eu^{3+} - doped

multicomponent tellurite glasses, Optical Materials, 70, 31 – 40, (2017).

124. O. Ravi, C. Madhukar Reddy, B. Sudhakar Reddy, B. Deva Prasad Raju, Judd – Ofelt analysis and spectral properties of Dy^{3+}- ions doped niobium containing tellurium calcium zinc borate glasses, Optics Communications, 312, 263 – 268, (2014).
125. M. V. Vijaya Kumar, K. Rama Gopal, R. R. Reddy, G. V. Lokeswara Reddy, N. Sooraj Hussain, B. C. Jamalaiah, Application of modified Judd – Ofelt theory and the evaluation of radiative properties of Pr^{3+} - doped lead telluroborate glasses for laser applications, Journal of Non – Crystalline Solids, 364, 20 – 27, (2013).
126. B. C. Jamalaiah, M. V. Vijaya Kumar, K. Rama Gopal, Investigation on luminescence and energy transfer in Tb^{3+} - doped lead telluroborate glasses, Physica B, 406, 2871 – 2875, (2011).
127. Yuan Gao, Qiu – Hua Nie, Tie – Feng Xu, Xiang Shen, Study of luminescence properties of novel Er^{3+} single – doped and Er^{3+} / Yb^{3+} co – doped tellurite glasses,Spectrochimica Acta Part A, 61, 1259 – 1262, (2005).
128. F. Fusari, S. Vetter, A. A. Lagatsky, B. Richards, S. Calvez, A. Jha, M. D. Dawson, W. Sibbert, Tunable laser operation of a Tm^{3+} - doped tellurite glass laser near 2 μm pumped by a 1211 nm semiconductor disk laser, Optical Materials, 32, 1007 – 1010, (2010).

129. I. Iparraguirre, J. Azkargorta, J. M. Fernandez – Navarro, M. Al – Saleh, J. Fernandez, R. Balda, Laser action and upconversion of Nd^{3+} in tellurite bulk glass, Journal of Non – Crystalline Solids, 353, 990 – 992, (2007).
130. Vu Phi Tuyen, Vu Xuan Quang, Phan Van Do, Luong Duy Thanh, Nguyen Xuan Ca, Vu Xuan Hoa, Le Van Tuat, Le Anh Thi, Masayuki Nogami, An in – depth study of the Judd – Ofelt analysis, spectroscopic properties and energy transfer of Dy^{3+} in alumino – lithium – telluroborate glasses, Journal of Luminescence , 210, 435 – 443 , (2019).
131. M. K. Halimah, M.F. Faznny, M. N. Azlan, H. A. A. Sidek, Optical basicity and electronic polarizability of zinc borotellurite glass doped La^{3+} ions, Results in Physics, 7, 581 – 589, (2017).
132. Kamal Damak, El Sayed Yousef, Christian Russel, Ramzi Maalej, White light generation from Dy^{3+} doped tellurite glass, Journal of Quantitative Spectroscopy & Radiative Transfer, 134, 55 – 63, (2014).
133. Salah Hassan Alazoumi, Sidek Abdul Aziz, R. El – Mallawany, Umar Sa'ad Aliyu, Halimah Mohamed Kamari, Mohd Hafiz Mohd Zaid, Khamirul Amin Matori, AbdulbasetUshah, Optical properties of zinc lead tellurite glasses, Results in Physics, 9, 1371 – 1376, (2018).
134. K. A. Naseer, S. Arunkumar, K. Marimuthu, The impact of Er^{3+}ions on the spectroscopic scrutiny of Bismuth barium telluroborate glasses for display devise and 1.53

μm amplification, Journal of Non – Crystalline Solids, 520, 119463, (2019).

135. K. Maheshvaran, K. Marimuthu, Comcentration dependent Eu^{3+} doped boro – tellurite glasses – Structural and optical investigations, Journal of Luminescence, 132, 2259 – 2267, (2012).
136. Ning Lei, Bing Xu, Zhonghong Jiang, Ti: sapphire laser pumped Nd: tellurite glass laser, Optics Communications, 127, 263 – 265, (1996).
137. Kefeng Li, Guang Zhang And Lili Hu, Watt – level ~ 2 μm laser output in Tm^{3+}- doped tungsten tellurite glass double – cladding fiber, Optics Letters, Vol. 35, No. 24, (2010).
138. Mira Naftaly, Shaoxiong Shen and Animesh Jha, Tm^{3+} - doped tellurite glass for a broadband amplifier at 1.47 μm, Applied Optics, Vol. 39, No. 27, (2000).
139. Xiang Peng, Feng Song, Shibin Jiang and N. Peyghambarian, Makoto Kuwata – Gonokami, Lei Xu, Fiber – taper – coupled L – band Er^{3+} - doped tellurite glass microsphere laser, Applied Physics Letters, Vol. 82, No. 10, (2003).
140. Xiang Peng, Feng Song, Makoto Kuwata – Gonokami, Shibin Jiang and N. Peyghambarian, Temperature dependence of the wavelength and threshold of fiber – taper – coupled L – band Er^{3+} - doped tellurite glass microsphere laser, Applied Physics Letters, Vol.83, No. 26, (2003).

141. Billy Richards, Shaoxiong Shen, Animesh Jha, Yuen Tsang, David Binks, Infrared emission and energy transfer in Tm^{3+}, Tm^{3+} - Ho^{3+} and Tm^{3+} - Yb^{3+} - doped tellurite fiber, Optics Express 6546, Vol. 15, No. 11, (2007).
142. F. Fusari, A. A. Lagatsky, B. Richards, A. Jha, W. Sibbett and C. T. A. Brown, Spectroscopic and lasing performance of Tm^{3+} - doped bulk TZN and TZNG tellurite glasses operating around 1.9 μm, Optics Express 19146, Vol. 16, No. 23, (2008).
143. Kefeng Li, Guang Zhang, Xin Wang, Lili Hu, PeiwenKuan, Danping Chen and Meng Wang, Tm^{3+} and Tm^{3+} - Ho^{3+} co – doped tungsten tellurite glass single mode fiber laser, Optics Express 10115, Vol. 20, No. 9, (2012).
144. Billy Richards, Yuen Tsang, David Binks, Joris Lousteau and Animesh Jha, Efficient ~ 2 μm Tm^{3+} - doped tellurite fiber laser, Optics Letters, Vol. 33, No. 4, (2008).
145. S. Arunkumar, K. Annapoorani and K. Marimuthu, Investigations on Optical Properties of Eu^{3+} ion Doped Magnesium Telluroborate Glasses for Red Laser Applications, DAE Solid State Physics, Symposium (2017).
146. Hssen Fares, Habib Elhouichet, Bernard Gelloz, and Mokhtar Ferid, Silver nanoparticles enhanced luminescence properties of Er^{3+} doped tellurite glasses: Effect of heat treatment, Journal of Applied Physics 116, 123504, (2014).

147. Manal Abdel – Baki, Fouad El – Diasty, Glasses for Photonic Technologies, International Journal of Optics and Applications, 3(6), 125 – 137, (2013).
148. S. Pravinraj, M. Vijaykumar, K. Marimuthu, Enhanced luminescence behavior of Eu^{3+} doped heavy metal oxide telluroborate glasses for Laser and LED applications, Accepted Manuscript.
149. Purushottam Joshi, Billy Richards and Animesh Jha, Reduction of OH^- ions in tellurite glasses using chlorine and oxygen gases, Journal of Materials Research 28 (23), 3226 – 3233, (2013).
150. K. Selvaraju, K. Marimuthu, Structural and Spectroscopic studies on Concentration dependent Sm^{3+} doped Boro – tellurite glasses, Accepted Manuscript.
151. D. DOROSZ, Rare earth ions doped aluminosilicate and phosphate double clad optical fibers, Technical Science, Vol. 56, No. 2. (2008).
152. J. S. Wang, E. M. Vogel, E. Snitzer, Tellurite glass: a new candidate for fiber devices, Optical Materials 3, 187 – 203, (1994).
153. A. K. YAKHKIND, Tellurite glasses, Journal of The American Ceramic Society, Vol. 49, No. 12, (1996).
154. Jianhu Yang, Liyan Zhang, Lei Wen, ShixunDai, Lili Hu and Zhonghong Jiang, Optical transitions and upconversion luminescence of Er^{3+}/ Yb^{3+} - codoped halide modified tellurite glasses, Journal of applied Physics, Vol. 95, No. 06, (2004).

155. Shiqing Xu, Zhongmin Yang, Guonian Wang, Junjie Zhang, Shixun Dai, Lili Hu, Zhonghong Jiang, Effects of chloride introduction on up – conversion luminescence in Tm^{3+} - doped tellurite glasses, Spectrochimica Acta Part A, 60, 3025 – 3028, (2004).
156. Xiushan Zhu and N. Peyghambarian, High – Power ZBLAN Glass Fiber Lasers: Review and Prospect, Advances in OptoElectronics, Vol. 2010, 501956, 23, (2010).
157. FiorenzoVetrone, John – Christopher Boyer, and John A. Capobianco, Adolfo Speghini and Macro Bettinelli, 980 nm excited upconversion in an Er – doped ZnO – TeO_2 glass, Applied Physics Letters, Vol. 80, No. 10, (2002).
158. Pham Van Hoi, Chu Thi Thu Ha, and Hoang Quang Hung, Long – band emission of microsphere lasers based on erbium – doped sol – gel silica – alumina glasses, Applied Physics Letters, 87, 161110, (2005).
159. Hiroki Yamauchi, Ganapathy Senthil Murugan, and YasutakeOshishi, Optical properties of Er^{3+} and Tm^{3+} ions in a tellurite glass, Journal of Applied Physics, 97, 043505, (2005).
160. Anant Kumar Singh, Garima Tripathi and S. B. Rai, Anita Rai, Enhancement of upconverted luminescence in Er^{3+}: TeO_2 glass on increasing the temperature and concentration of Yb^{3+} beyond the critical limit, Journal of Applied Physics, 101, 103105, (2007).
161. V. Uma, K. Maheshvaran, K. Marimuthu, G. Muralidharan, Structural and optical investigations on

Dy^{3+} doped lithium tellurofluoroborate glasses for white light applications, Journal of Luminescence, 176, 15 – 24, (2016).

162. M. V. Vijay Kumar, B. C. Jamalaiah, K. Rama Gopal, R. R. Reddy, Novel Eu^{3+} - doped lead telluroborate glasses for red laser source applications, Journal of Solid State Chemistry, 184, 2145 – 2149, (2011).
163. M. V.Vijayakumar, B. C. Jamalaiah, K. Rama Gopal, R. R. Reddy, Optical aborption and fluorescence studies of Dy^{3+} - doped lead telluroborate glasses, Journal of Luminescence,132, 86 – 90, (2012).
164. M. V. Vijaya Kumar, K. Rama Gopal, R. R. Reddy, G. V. Lokeswara Reddy, B. C. Jamalaiah, Luminescence and gain characteristics of 1.53 μm broadband of Er^{3+} in lead telluroborate glasses, Journal of Luminescence, 142, 128 – 134, (2013).
165. P. Suthanthirakumar, P. Karthikeyan, P. K. Manimozhi, K. Marimuthu, Structural and spectroscopic behavior of Er^{3+}/ Yb^{3+} co – doped boro – tellurite glasses, Journal of Non – Crystalline Solids, 410, 26 – 34, (2015).
166. Phan Van Do, Vu Phi Tuyen, Vu Xuan Quang, Le Xuan Hung, Luong Duy Thanh, Tran Ngoc, Ngo Van Tam, Bui The Huy, Investigation of spectroscopy and the dual energy transfer mechanisms of Sm^{3+} - doped telluroborate glasses, Optical Materials, 55, 62 – 67, (2016).
167. V. Uma, K. Marimuthu, G. Muralidharan, Influence of Modifier Cations on the Spectroscopic Properrties of

Dy^{3+} Doped Telluroborate Glasses for White Light Applications, J. Fluoresc, Springer, 10.1007,(2016).

168. Zizhong Zhou, Yaxun Zhou, Pan Cheng, Effect of B_2O_3 addition on luminescent properties and energy transfer in Er^{3+}/ Ho^{3+} - codoped tellurite glasses, Journal of Alloys and Compounds, 717, 141 – 149, (2017).
169. V. Uma, M. Vijayakumar, K. Marimuthu, G. Murlidharan, Luminescence and energy transfer studies on Sm^{3+}/ Tb^{3+}codopedtelluroborate glasses for WLED applications, Journal of Molecular Structure, 1151, 266 – 276, (2018).
170. V. Uma, K. Marimuthu, G. Muralidharan, Effect of modifier oxides (SrO, Al_2O_3, ZnO, CdO, PbO and Bi_2O_3) on the luminescence properties of Er^{3+} doped telluroborate glasses for laser and optical amplifier applications, Journal of Luminescence, 207, 534 – 544, (2019).
171. Vu Phi Tuyen, Vu Xuan Quang, Phan Van Do, Luong Duy Thanh, Nguyen Xuan Ca, Vu Xuan Hoa, Le Van Tuat, Le Anh Thi, Masayuki Nogami, An in – depth study of the Judd – Ofelt analysis, Spectroscopic properties and energy tranfer of Dy^{3+} in alumino – lithium – telluroborate glasses, Jornal of Luminescence, 210, 435 – 443, (2019).
172. H O Tekin, Shams A M Issa, E. Kavaz,, and E EAltunsoy Guclu, The direct effect of Er_2O_3 on bismuth barium telluro borate glasses for nuclear security applications, Materials Research Express, 6, 115212, (2019).